ESTIMATING OVERBURDEN THICKNESS IN RESISTIVE AREAS FROM ON-TIME AIRBORNE EM DATA

By

Thomas Bagley

A thesis submitted in partial fulfillment
of the requirements for the degree of
Master of Science (MSc) in Geology

The Faculty of Graduate Studies
Laurentian University
Sudbury, Ontario, Canada

THESIS DEFENCE COMMITTEE/COMITÉ DE SOUTENANCE DE THÈSE
Laurentian Université/Université Laurentienne
Faculty of Graduate Studies/Faculté des études supérieures

Title of Thesis Titre de la thèse	Estimating overburden thickness in resistive areas from on-time airborne EM data
Name of Candidate Nom du candidat	Bagley, Thomas
Degree Diplôme	Master of Science
Department/Program Département/Programme	Geology
Date of Defence Date de la soutenance	September 27, 2019

APPROVED/APPROUVÉ

Thesis Examiners/Examinateurs de thèse:

Dr. Richard Smith
(Supervisor/Directeur(trice) de thèse)

Dr. Mostafa Naghizadeh
(Committee member/Membre du comité)

Robert Hearst
(Committee member/Membre du comité)

Dr. Mark Everett
(External Examiner/Examinateur externe)

Approved for the Faculty of Graduate Studies
Approuvé pour la Faculté des études supérieures
Dr. David Lesbarrères
Monsieur David Lesbarrères
Dean, Faculty of Graduate Studies
Doyen, Faculté des études supérieures

ACCESSIBILITY CLAUSE AND PERMISSION TO USE

Abstract

We propose a method to invert two-component time-domain EM data to a thick-sheet over half-space model, as a solution representing an overburden on top of bedrock. We first estimated the conductivity of the lower half-space using a combination of inversion for half-space (if appropriate) or a thin sheet over half-space (also when appropriate). This yielded a number of estimates, which could be combined to give a reasonable estimate of the lower half-space conductivity for the survey area. With this estimation an equation solver was used to solve the thick-sheet over half-space model for sheet thickness and sheet conductivity. The output of the algorithm was generally stable when applied to GEOTEM data in an area of moderately resistive overburden over a generally more resistive half-space. Although it did not reliably reproduce the overburden thicknesses as measured in the reference drill holes, it did give an estimate that was reasonable in the conductive areas.

Keywords:

Geophysics, electromagnetism, inversion, Athabasca, uranium

Acknowledgments

I'm profoundly grateful for the support of my supervisor Dr Richard Smith and for friendly mentorship. Richard gave me the head start, the Geophysics, and without him this work would not have been possible. I would also like to thank my external reviewer and thesis committee members Dr Mark Everrett, Rob Hearst, and Dr Mostafa Naghizadeh for taking the time to review the thesis; their comments were invaluable. Along the way I have also had help from Alan King and Ben Polzer, from whom I learned skills and concepts that improved this work. I must acknowledge the personal support that I have had from my parents Andrew and Christine over the years, because my achievements could just as well be theirs. Finally I would like to acknowledge the support of my loving girlfriend Dakota, my brother James for inspiring my imagination, and my fellow students.

Table of Contents

List of Figures

List of Tables

Chapter 1

1 Introduction and background

Active-source electromagnetic prospecting systems use a primary current flowing in a transmitter so as to excite the ground with a corresponding primary field Grant and West (1965). When this primary field varies as a function of time, secondary fields are induced in conductive bodies below the ground. This induced secondary field varies between two limits determined by the value of the dimensionless induction number, which is the product of the square of a critical dimension (size), the conductivity, magnetic permeability, and the frequency (or inverse time). When the induction number is high, this is the inductive limit and secondary currents that are generated oppose the change in the exciting primary field according to Faraday's law. This inductive-limit secondary field is entirely in phase with the primary field. At very small values of the induction number, the secondary field is at the resistive limit sometimes called the low-induction-number (LIN) regime. At this limit, the secondary response is proportional to the time derivative of the primary field, which is entirely out of phase or quadrature phase. These resistive-limit fields vary so slowly there is no interaction between the secondary fields at the resistive limit Wait (1982). In between these two limits, there is an interaction between secondary currents, so the decay of a current close to the inductive limit will induce other secondary currents in conductive bodies. This results in a mixture of in-phase and

quadrature phase fields in frequency domain systems or in time-domain systems a response that decays during the off-time.

Traditional time-domain airborne electromagnetic survey (AEM) interpretation methods use only the off-time response, which are measurements of the secondary field as it decays after the transmitter has been turned off. In highly resistive areas, the off-time response is effectively zero and interpretation cannot be applied. In the off-time, as shown by Grant and West (1965), the response of a thin conductive layer depends on the product of the conductivity-thickness (σt), so that the off-time response of a conductive overburden 30 m thick with a conductivity of 1 S/m could not be distinguished from an overburden 15 m thick with a conductivity of 2 S/m. A unique solution for the thickness or layer conductivity is not possible in this scenario using the off-time method.

On-time measurements are quadrature measurements made while the primary transmitter is active, and in resistive areas can be well above noise levels Smith (2001), and has been observed with existing AEM system configurations Annan et al. (1996). In resistive areas, the on-time is at the resistive limit, where there are different formulae for the response in the ρ or z component directions for both the thin-sheet and half-space models Smith and Lee (2002). By measurement of both the ρ and z components at the resistive limit, the fit of a thin-sheet or half-space model can be validated by the agreement or disagreement of their respective conductance and conductivity. If neither of these cases are appropriate, then the response of a thick-sheet above a half-space can be determined using a sum of thin sheet models as shown by McNeill (1980) and Wait (1982).

The resistive-limit data can also be estimated from frequency-domain systems by interpreting the quadrature response at low frequencies. Annan et al. (1996) have shown how the ρ-component response can be converted to a half-space conductivity; while Smith (2000) showed that the $\rho-$ and $z-$ resistive limits can be converted to an apparent conductivity-thickness product (conductance). For these simple cases the $\rho-$component and $z-$component estimates are independent and might be inconsistent if the model is not a half-space or thin-sheet. In this contribution we show how the $\rho-$ and $z-$ components can together be used to derive the thickness and conductivity of a thick-sheet above a half-space that is either highly resistive or has an estimated or assumed conductivity.

The method is tested on synthetic data and on field data collected in the Athabasca Basin of Saskatchewan using the GEOTEM system. This area is challenging, as the overburden and half-space are resistive, so the data is relatively noisy.

Chapter 2

2 Theory

The thin sheet and half space derivations presented in this section closely follow and use the same notation as is presented in Annan et al. (1996). The airborne EM system comprises a transmitter (T_x) positioned at an altitude ($z = h$), above the ground. In the following the transmitter is a vertical-axis dipole and the electromagnetic receiver (R_x) is comprised of two dipolar induction coils with the dipoles oriented horizontally and vertically (parallel to the ρ and z axes respectively). The receiver coils are positioned a radial distance ($\rho = X$) behind the aircraft and distance D vertically below the aircraft ($z = h - D$).

The primary field of the transmitter and excited secondary field can be expressed in terms of a magnetic Hertz potential, Π. For the case of a vertical-axis transmitter dipole, as is commonly used in airborne systems, the Hertz potential has only a vertical component. The total Hertz potential is the sum of the primary and secondary:

$$\Pi = \Pi_p + \Pi_s, \tag{1}$$

where for a unit dipole the primary field potential is Wait (1982)

$$\Pi_p = \frac{1}{4\pi r} s(t) \tag{2}$$

and the secondary field potential is

$$\Pi_s = \frac{1}{2\pi}\int_{-\infty}^{\infty} S(\omega)e^{i\omega t}\left[\int_0^{\infty}\frac{1}{4\pi}R(\lambda)e^{-\lambda(z+h)}J_0(\lambda\rho)\,\mathrm{d}\lambda\right]\mathrm{d}\omega. \tag{3}$$

A table of symbols for the above equations can be found in Table 1.

Details on the above formulation can be found in Wait (1982) or Ward (1966).

The radial, H_ρ, and vertical, H_z, components of the magnetic field are expressed as

$$H_\rho = \frac{\partial^2\Pi}{\partial\rho\partial z}, \tag{4}$$

$$H_z = \frac{\partial^2\Pi}{\partial z^2}. \tag{5}$$

The radial and vertical primary fields are

$$H_\rho^P(t) = \frac{-3\rho(z-h)}{4\pi\left(\rho^2+(z-h)^2\right)^{5/2}}s(t), \tag{6}$$

and

$$H_z^P(t) = \frac{2(z-h)^2-\rho^2}{4\pi\left(\rho^2+(z-h)^2\right)^{5/2}}s(t), \tag{7}$$

ω	angular frequency
λ	horizontal wavenumber
μ	constant magnetic permeability
σ_n	electrical conductivity of the nth layer
i	$(-1)^{\frac{1}{2}}$
$k_n^2 = (i\omega\mu\sigma_n)$	propagation constant in the nth layer
$\gamma_n = (\lambda^2 - k_n^2)^{1/2}$	vertical wavenumber in the nth layer
$R(\lambda) = \frac{\lambda - u_1}{\lambda + u_1}$	half-space transverse-electric (TE) reflection coefficient
$u_1 = \gamma_1 \frac{\gamma_2 + \gamma_1 \tanh(\gamma_1 d_1)}{\gamma_1 + \gamma_2 \tanh(\gamma_1 d_1)}$	recursion formula for u in the top layer
d_1	thickness of the top layer
$r = (\rho^2 + (z-h)^2)^{1/2}$	distance between transmitter and receiver
$s(t)$	transmitter current waveform
$S(\omega)$	transmitter current spectrum

Table 1: Table of symbols.

Chapter 3

3 Resistive limit analytical solutions

In the resistive limit, the frequency is sufficiently low that eddy-current self interaction is negligible Annan et al. (1996). Formally, this is written mathematically as $|\gamma_i/\lambda^2| << 1$.

3.1 The conductive sheet model

If the conductivity of the second-layer is zero and the thickness d_1 of the top layer is vanishingly small (while the conductivity thickness product is finite) then

$$\begin{aligned} \gamma_2 &= \lambda \\ u_1 &= \lambda - i\omega\mu\sigma d_1, \end{aligned} \tag{8}$$

Wait (1982). The reflection coefficient therefore simplifies to

$$R(\lambda) = \frac{i\omega\mu\sigma d_1}{2\lambda}. \tag{9}$$

Taking the derivative with respect to z of the secondary Hertz potential, then the term in square brackets on the right-hand-side of equation 3 can be integrated using the Lipschitz related integrals Wait (1982) to give the frequency-domain expression

$$\frac{\partial \Pi_S}{\partial z} = \frac{-i\omega\mu\sigma d_1}{8\pi\sqrt{\rho^2 + (z+h)^2}}. \tag{10}$$

From equations 10 and 4 and 5 we can write

$$H_\rho^S = \frac{i\omega\mu\sigma d_1 \rho}{8\pi\left[\rho^2 + (z + h^2)\right]^{3/2}} \tag{11}$$

and

$$H_z^S = \frac{i\omega\mu\sigma d_1 (z+h)}{8\pi\left[\rho^2 + (z+h)^2\right]^{3/2}}. \tag{12}$$

In both cases the secondary field is quadrature phase and exhibits the well known linear increase with frequency. The $i\omega$ factor in the frequency domain transforms to a time derivative in the time domain, so in the time domain equations 11 and 12

become

$$H_\rho^s(t) = \frac{\mu\sigma d_1}{8\pi}\left[\frac{\rho}{(\rho^2+(z+h)^2)^{3/2}}\right]\frac{\mathrm{d}s(t)}{\mathrm{d}t}, \tag{13}$$

$$H_\rho^s(t) = \frac{\mu\sigma d_1}{8\pi}\left[\frac{(z+h)}{(\rho^2+(z+h)^2)^{3/2}}\right]\frac{\mathrm{d}s(t)}{\mathrm{d}t}. \tag{14}$$

This result shows that at the resistive limit, there is no off-time response as ds/dt is zero in the off time. Most importantly, the response is proportional to the conductivity-thickness product σd_1.

Typical AEM systems use induction coil sensors, which measure a voltage that is proportional to the time rate of change of the magnetic flux, $V = -\partial\phi/\partial t$, where the flux $\phi = AB$ and B is the magnitude of the magnetic flux density cutting the coil and A is the area of the receiver coil. As $\mathbf{B} = \mu\mathbf{H}$, then the voltage measured in the coil is

$$V_i^j = \sigma d_1 G_i(z,\rho,h)\frac{d^2 s(t)}{dt^2}\,, \tag{15}$$

where the subscript i denotes the component and the relevant formula for the G_i are

$$G_\rho(z,\rho,h) = \frac{\mu^2 A}{8\pi}\left[\frac{\rho}{(\rho^2+(z+h)^2)^{3/2}}\right]\,, \tag{16}$$

$$G_z(z,\rho,h) = \frac{\mu^2 A}{8\pi}\left[\frac{(z+h)}{(\rho^2+(z+h)^2)^{3/2}}\right]\,, \tag{17}$$

and for the airborne systems $\rho = X$ and $z = h - D$.

Since the GEOTEM and MEGATEM waveforms can be represented by a half-sine

pulse, that starts at $t = 0$ and ends at $t = P$, viz.

$$s(t) = S_0 \sin(\pi t/P) \tag{18}$$

during the pulse and $s(t) = 0$ elsewhere. The maximum dipole moment is in the middle of the pulse at $t = P/2$ and has a magnitude of S_0 and units of Am^2. Differentiating this once, we get

$$\frac{ds(t)}{dt} = S_0 \frac{\pi}{P} \cos(\pi t/P) \left(u(t) - u(t-P)\right) , \tag{19}$$

where the $u(t)$ is the unit step-on function (unit for positive argument), here being used to ensure that the derivative of the dipole moment waveform is non-zero (on) between $t = 0$ and $t = P$. Differentiating this again, we get

$$\frac{d^2 s(t)}{dt^2} = S_0 \left[\frac{\pi}{P} \cos(\pi t/P) \left(\delta(t) + \delta(t-P)\right) - \left(\frac{\pi}{P}\right)^2 \sin(\pi t/P) \left(u(t) - u(t-P)\right) \right] , \tag{20}$$

where $\delta(t)$ is the dirac delta function. From this we can see that the earth response in the resistive limit is a large spike at the switch on and the switch off of the transmitter pulse at $t = 0$ and $t = P$ and a half sine function between Annan et al. (1996). Consequently the initial on-time measurement window used with the GEOTEM and MEGATEM was placed at the start of the waveform centred on t=0. Integrating expression 20 over a window of width ε, centred at time t=0 yields the

required on-time response,

$$O_i = \frac{1}{\varepsilon} \int_{-\varepsilon/2}^{\varepsilon/2} V_i(t)\, dt\,, \tag{21}$$

$$= \frac{\sigma d_1 \pi G_i S_0}{\varepsilon P}\,. \tag{22}$$

The resulting expression can be rearranged to give the conductance of the thin sheet

$$\sigma d_1 = \frac{\varepsilon P O_i}{\pi G_i S_0}. \tag{23}$$

To ensure that the resultant expression has the units of Siemens, the ε and P must be in seconds, O_i in volts, G_i in $\mathrm{kg^2 s^{-4} A^{-4} m^2}$ and S_0 in $\mathrm{Am^2}$. The GEOTEM and MEGATEM voltage responses are often reported in $\mathrm{pV/m^2}$, which is the voltage already divided by the area of the receiver coil, making this effectively a receiver coil with a unit area. Hence the A in expressions (16) or (17) should be set to 1 $\mathrm{m^2}$ and the voltage in $\mathrm{pV/m^2}$ should be converted to $\mathrm{V/m^2}$.

Since the geologic setting will seldom truly be a thin sheet, the name "on-time apparent conductance" is used. The thin sheet will not always lie at the surface or be above a highly resistive half-space, so the estimate of the conductance $S_\rho = \sigma d_1$ from the ρ component and the conductance $S_z = \sigma d_1$ from the z component will in these cases not be equal. If we assume that the half-space has a zero conductivity and set $S_\rho = S_z$ and solve for a new value for the sum of the T_x and R_x height giving

$$h = \rho \frac{O_z}{O_\rho}\,, \tag{24}$$

which allows us to solve for h the altitude of the transmitter above the thin sheet. Substituting back into equation (23) using either the ρ or z component should give the same value of conductance from both components. If the altitude is significantly less than the altimeter reading, then the model is obviously inappropriate. If the altitude is too large, then it is possible that a better model could be used.

3.2 Half-space model

If the model is a half-space, then

$$\begin{aligned} d_1 &= 0, \\ u_1 &= \gamma_1. \end{aligned} \tag{25}$$

At the resistive limit, the reflection coefficient becomes

$$R(\lambda) \approx \frac{i\omega\mu\sigma}{4\lambda^2}, \tag{26}$$

which again allows the field expressions to be integrated analytically using the Lipschitz integrals as discussed by Wait (1982), giving the following expression for H_ρ and H_z frequency-domain responses

$$H_\rho^S(\omega) = \frac{i\omega\mu\sigma}{16\pi\rho}\left[1 - \frac{z+h}{(\rho^2+(z+h)^2)^{1/2}}\right], \tag{27}$$

$$H_z^S(\omega) = \frac{i\omega\mu\sigma}{16\pi}\left[\frac{1}{(\rho^2+(z+h)^2)^{1/2}}\right], \tag{28}$$

which become on transformation to the time domain

$$H_\rho^S(t) = \frac{\mu\sigma}{16\pi\rho}\left[1 - \frac{z+h}{(\rho^2+(z+h)^2)^{1/2}}\right]\frac{\mathrm{d}s(t)}{\mathrm{d}t}, \tag{29}$$

$$H_z^S(t) = \frac{\mu\sigma}{16\pi}\left[\frac{1}{(\rho^2+(z+h)^2)^{1/2}}\right]\frac{\mathrm{d}s(t)}{\mathrm{d}t}. \tag{30}$$

Note once again that there is no response in the off-time and the response is proportional to the half-space conductivity.

Proceeding similarly to the conductive sheet model, we can write

$$\sigma = \frac{\varepsilon PO_i}{\pi G_i S_0} \tag{31}$$

where

$$G_\rho^H(z,\rho,h) = \frac{\mu^2 A}{16\pi\rho}\left[1 - \frac{z+h}{(\rho^2+(z+h)^2)^{1/2}}\right], \tag{32}$$

$$G_z^H(z,\rho,h) = \frac{\mu^2 A}{16\pi}\left[\frac{1}{(\rho^2+(z+h)^2)^{1/2}}\right], \tag{33}$$

and for the airborne systems $\rho = X$ and $z = h - D$.

Once again the ρ and z components can be used to give the half-space apparent conductivity. However, there is no guarantee that the values obtained will be the same. It is possible to show that the ρ and z components will give a consistent value if

$$z + h = \frac{\rho^2 + \alpha^2}{2\alpha},$$

where

$$\alpha = \frac{O_\rho}{O_z}.$$

3.3 Thin sheet overlying a half-space model

If the model is comprised of a thin conductive sheet at the surface overlying a conductive half-space then at the resistive limit

$$u_1 = \sqrt{\lambda^2 - i\omega\mu\sigma_2} - i\omega\mu\sigma_1 d_1, \tag{34}$$

and

$$R(\lambda) = \frac{i\omega\mu\sigma_2}{4\lambda^2} + \frac{i\omega\mu\sigma_1 d_1}{2\lambda}. \tag{35}$$

By inspection, the reflection coefficient is the sum of the thin-sheet and half-space reflection coefficients, so the measured response can be written

$$\begin{aligned} \frac{\epsilon P O_\rho}{\pi S_0} &= \sigma_1 d_1 G_\rho^{TS} + \sigma_2 G_\rho^H, \\ \frac{\epsilon P O_z}{\pi S_0} &= \sigma_1 d_1 G_z^{TS} + \sigma_2 G_z^H, \end{aligned} \tag{36}$$

where the superscripts TS and H denote the geometry factors for the thin-sheet and half-space equations (16), (17) and (32), (33), respectively. This is a linear system of equations, the solution to which is

$$\begin{pmatrix} \sigma_1 d_1 \\ \sigma_2 \end{pmatrix} = \frac{1}{G_\rho^{TS} G_z^H - G_z^{TS} G_\rho^H} \begin{pmatrix} G_z^H & -G_\rho^H \\ -G_z^{TS} & G_\rho^{TS} \end{pmatrix} \begin{pmatrix} \frac{\varepsilon O_\rho P}{\pi S_0} \\ \frac{\varepsilon O_z P}{\pi S_0} \end{pmatrix}. \tag{37}$$

Valid solutions to this inversion will have the conductance and the conductivity positive.

Chapter 4

4 Sensitivity Analysis

A half-space sensitivity analysis is performed for the purposes of determining the contribution of the material at each depth to the response and hence the apparent conductivity.

If the substitution

$$u_1 = \frac{1}{Q} \tag{38}$$

is made, then

$$R(\lambda) = \frac{\lambda Q - 1}{\lambda Q + 1}, \tag{39}$$

and

$$\frac{\partial R(\lambda)}{\partial Q} = \frac{2\lambda}{(\lambda Q + 1)^2}. \tag{40}$$

In the resistive limit, $u_1 \approx \lambda$, so

$$\frac{\partial R(\lambda)}{\partial Q} = \frac{\lambda}{2}. \tag{41}$$

The change in Q resulting from integrating small changes in the conductivity at

depth z' is

$$\delta Q = \int_0^\infty i\omega\mu \frac{e^{-2u_1 z'}}{u_1^2} \delta\sigma(z')\,\mathrm{d}z', \tag{42}$$

(Parker (1977); Edwards and Cheesman (1987); Smith et al. (1994)). If the resistive limit approximation is made and fractional changes in the conductivity are considered, then

$$\delta Q = \int_0^\infty i\omega\mu\sigma \frac{e^{-2\lambda z'}}{\lambda^2} \ln\sigma(z')\,\mathrm{d}z'. \tag{43}$$

The fractional change in $\partial \prod / \partial z$ is then

$$\begin{aligned} \delta\left(\partial\Pi/\partial z\right) &= \frac{\partial(\partial\Pi/\partial z)}{\partial Q}\delta Q \\ &= \frac{-i\omega\mu\sigma}{8\pi} \int_0^\infty e^{-\lambda(z+h)} J_0(\lambda\rho)\,\mathrm{d}\lambda \int_0^\infty e^{-2\lambda z'} \delta \ln\sigma(z')\,\mathrm{d}z'. \end{aligned} \tag{44}$$

As the only perturbation of interest is a unit fractional change in the conductivity at depth z', then $\delta \ln\sigma = \delta(z')$, where $\delta(z')$ is the Dirac delta function. Equation (44) thus becomes

$$\delta(\partial\Pi/\partial z) = \frac{-i\omega\mu\sigma}{8\pi} \left[\frac{1}{\sqrt{\rho^2 + (z+h+2z')^2}}\right], \tag{45}$$

which can be used to give the sensitivities for H_p and H_z using equations (4) and (5)

$$\delta H_\rho = \frac{i\omega\mu\sigma}{8\pi} \left[\frac{\rho}{[\rho^2 + (z+h+2z')^2]^{3/2}}\right], \tag{46}$$

$$\delta H_z = \frac{i\omega\mu\sigma}{8\pi} \left[\frac{z+h+2z'}{[\rho^2 + (z+h+2z')^2]^{3/2}}\right]. \tag{47}$$

Note that these are the formulae for the magnetic field of a thin sheet when z and h have been replaced by $z+z'$ and $h+z'$ respectively. This shows that in the resistive limit a unit fractional change in the conductivity at a depth z' is the same as the resistive-limit response of a thin sheet at the same depth. As the thin sheet is by definition surrounded by non-conducting material which it does not interact with, then the perturbation is not interacting with the other material in the half-space. The normalized sensitivities are

$$\frac{\delta H_\rho}{H_\rho} = \frac{2\rho^2}{[\rho^2+(z+h+2z')^2]^{3/2}\left[1-\frac{(z+h)}{(\rho^2+(z+h)^2)^{1/2}}\right]}, \tag{48}$$

and

$$\frac{\delta H_z}{H_z} = \frac{2(z+h+2z')\sqrt{\rho^2+(z+h)^2}}{[\rho^2+(z+h+2z')^2]^{3/2}}. \tag{49}$$

Defining scaled variables $z_s=(z+h)/\rho$ and $z_a=z'/\rho$, these become

$$\frac{\delta H_\rho}{H_\rho} = \frac{2}{\rho\,[1+(z_s+2z_a)^2]^{3/2}\left[1-\frac{z_s}{(1+z_s^2)^{1/2}}\right]}, \tag{50}$$

and

$$\frac{\delta H_z}{H_z} = \frac{2(z_s+2z_a)\sqrt{1+z_s^2}}{\rho\,[1+(z_s+2z_a)^2]^{3/2}}. \tag{51}$$

For the case when $z=h=0$, the latter of the two equations reduces to that given by McNeill (1980). These functions are plotted on Figure 1 for the case when $\rho=135$ m and $z+h$=185 m.

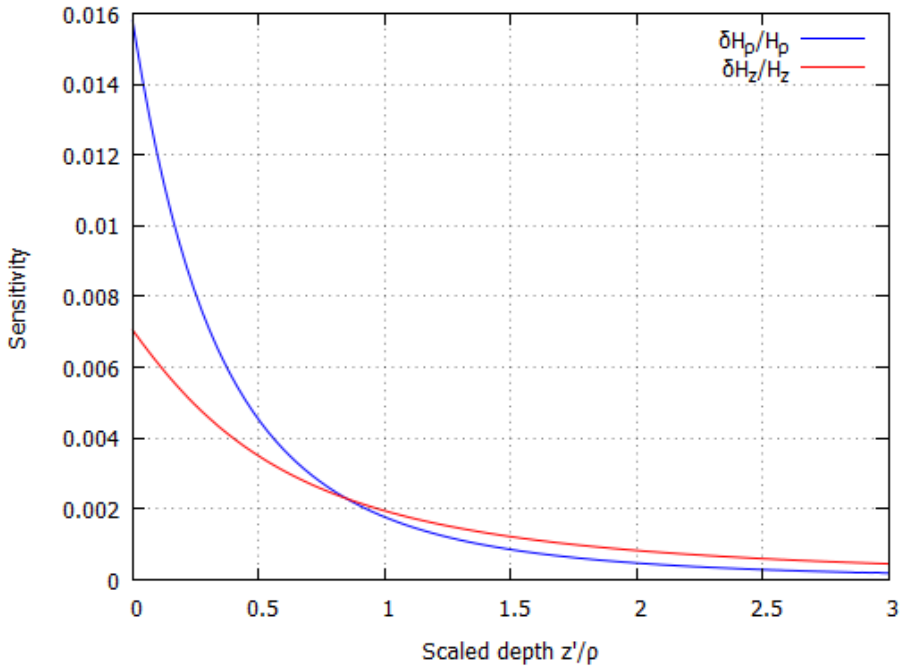

Figure 1: Sensitivity of ρ (blue) and z components (red) to changes in the conductivity of a half-space at a specific scaled depth.

The effect of the deeper material is illustrated by multiplying the sensitivity by the depth (Edwards and Cheesman (1987); Spies (1989); Smith et al. (1994)). Figure 2 shows the sensitivity in these circumstances.

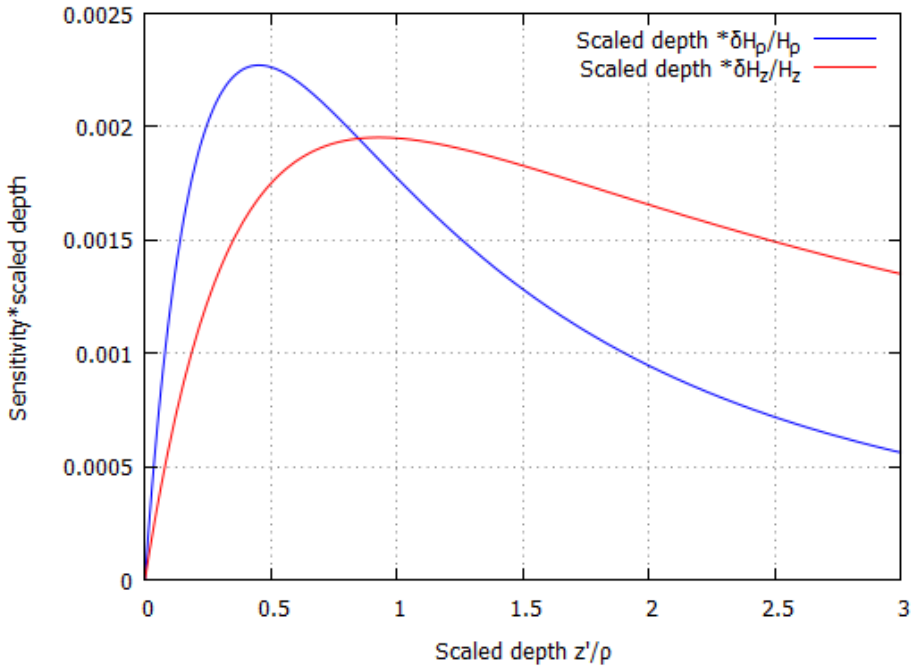

Figure 2: Sensitivity of the ρ (blue) and z components (red) to changes in the conductivity of a half-space at a specific scaled depth. In this case the sensitivity has been multiplied by the depth to emphasize depths with significant impact.

The depth at which the z and ρ components have equal sensitivities can be obtained by equating equations (50) and (51). This gives

$$z' = \rho z_a = \frac{\rho}{2}\sqrt{1+z_s^2}, \tag{52}$$

which is about 115 m for the standard configuration. The conductivity more strongly influences the ρ component at depths shallower than 115 m, the z component at depths greater than 115 m.

4.1 Model with two layers

An important function for interpreting the effect of subsurface conductivity is the cumulative response defined by McNeill (1980).

$$R_i(z') = \int_{z'}^{\infty} \frac{\delta H_i}{H_i}\,\mathrm{d}z, \tag{53}$$

where $i = \rho$ or z. For a two layer earth, the x- and z-component apparent conductivity can be written as the sum of the contribution of two non-interacting layers McNeill (1980). Integrated analytically his gives

$$R_\rho(z_a) = \frac{\left[1 - \frac{z_s+2z_a}{\sqrt{1+(z_s+2z_a)^2}}\right]}{\left[1 - \frac{z_s}{\sqrt{1+z_s^2}}\right]}, \tag{54}$$

$$R_z(z_a) = \frac{\sqrt{1+z_s^2}}{\sqrt{1+(z_s+2z_a)^2}}. \tag{55}$$

where z_s and z_a are defined before equation (50).

These functions have been plotted on Figure 3. McNeill (1980) defines the depth of exploration as the depth at which the cumulative response is equal to 0.3. From Figure 3 this gives scaled depths of 0.75 and 2.1 for the radial and vertical component respectively. For the standard geometry this corresponds to depths of 100 and 284 metres. More conservative estimates are the peak positions on Figure 2 which give scaled penetration depths of 0.5 and 1.0 (67 and 135 m respectively).

The power of the cumulative response function is that it can be used to relate the actual conductivity as a function of depth to the apparent conductivity. The re-

lationship exists because there is no mutual interaction between material at different depths.

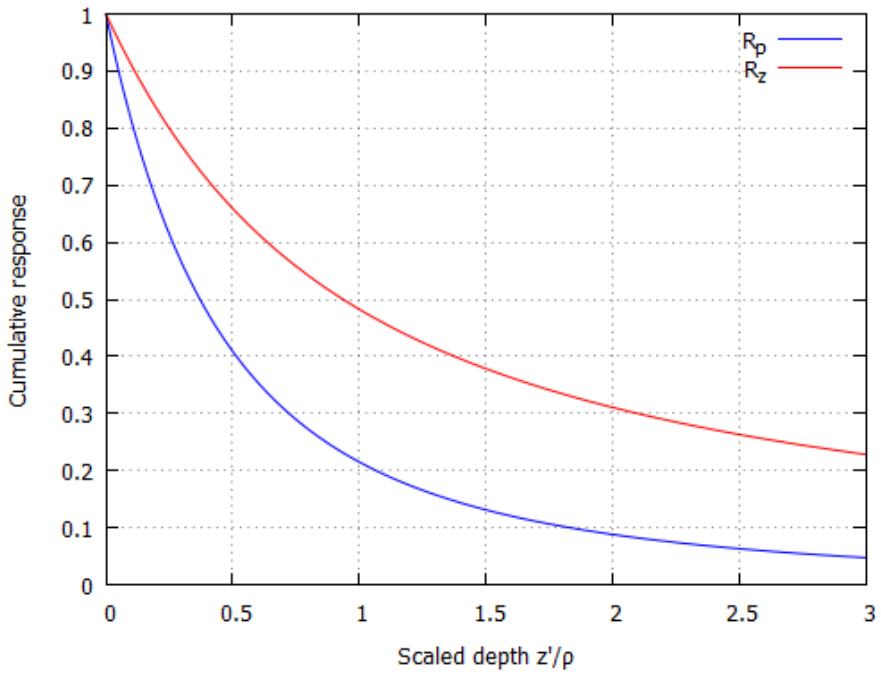

Figure 3: Cumulative response functions for the ρ component (blue) and the z component (red).

For a two layer earth, the ρ and z - component apparent conductivity can be written

$$\begin{aligned} \sigma_\rho^a &= \sigma_1 \left(1 - R_\rho(d_1)\right) + \sigma_2 R_\rho(d_1), \\ \sigma_z^a &= \sigma_1 \left(1 - R_z(d_1)\right) + \sigma_2 R_z(d_1), \end{aligned} \tag{56}$$

where σ_1 and d_1 are the conductivity and thickness of the top layer and σ_2 is the conductivity of the bottom layer. This is a set of two non-linear equations in three unknowns. Although it might be possible to use non-linear solvers to find non-unique solutions to these equations, we have chosen to solve these equations by making

intelligent assumptions about one of the parameters.

4.1.1 Thick sheet model

If the conductivity of the bottom layer is assumed to be zero, then σ_1 can be eliminated from (56) to give

$$f(d_1) = \frac{1 - R_\rho(d_1)}{1 - R_z(d_1)} - \frac{\sigma_\rho^a}{\sigma_z^a} = 0. \tag{57}$$

The first term of $f(d_1)$ is monotonically decreasing, so this equation can be solved with a simple root finder (e.g., Brent's method). However, a solution exists for a limited range of the ratio σ_ρ/σ_z. The first term goes to 1 as $d_1 \to \infty$; and as $d_1 \to 0$, the limiting value can be found by using a Taylor series expansion

$$\begin{aligned} \lim_{d_1 \to 0} \frac{1 - R_\rho(d_1)}{1 - R_z(d_1)} &= \frac{1 - \left(R_\rho(0) + d_1 \frac{\mathrm{d}R_\rho}{\mathrm{d}d_1}|_{d_1 \to 0} \right)}{1 - \left(R_z(0) + d_1 \frac{\mathrm{d}R_z}{\mathrm{d}d_1}|_{d_1 \to 0} \right)} \\ &= \frac{\frac{\mathrm{d}R_\rho}{\mathrm{d}d_1}|_{d_1 \to 0}}{\frac{\mathrm{d}R_z}{\mathrm{d}d_1}|_{d_1 \to 0}} \end{aligned} \tag{58}$$

From equations (54) and (55),

$$\frac{\mathrm{d}R_\rho}{\mathrm{d}z_a} = \frac{-2}{\left(1 - \frac{z_s}{\sqrt{1+z_s^2}} \right) \left(1 + (z_s + 2z_a)^2 \right)^{3/2}} \tag{59}$$

$$\frac{\mathrm{d}R_z}{\mathrm{d}z_a} = \frac{-2(z_s + 2z_a)\sqrt{1 + z_s^2}}{\left(1 + (z_s + 2z_a)^2 \right)^{3/2}} \tag{60}$$

which gives

$$\lim_{d_1 \to 0} \frac{1 - R_\rho(d_1)}{1 - R_z(d_1)} = \frac{1}{z_s \sqrt{1 + z_s^2} - z_s^2}. \tag{61}$$

for the normal geometry, this limiting value is equal to 2.24. Thus, for a thick sheet solution to exist, it is required that

$$1 \leq \sigma_\rho / \sigma_z \leq 2.24. \tag{62}$$

Once d_1 has been found by solving (57), σ_1 can be found by substituting into either of the equations in (56).

4.1.2 Known thickness

If the thickness is known, assumed, or selected from equation (52), then the equations in (56) reduce to a set of linear equations, the solution to which is

$$\begin{pmatrix} \sigma_1 \\ \sigma_2 \end{pmatrix} = \frac{1}{R_z - R_\rho} \begin{pmatrix} R_z & -R_\rho \\ -(1 - R_z) & 1 - R_\rho \end{pmatrix} \begin{pmatrix} \sigma_\rho \\ \sigma_z \end{pmatrix}. \tag{63}$$

This equation is non-singular unless $R_z = R_\rho$. This only occurs when $R_z = R_\rho = 1$, in which case the ground is a half-space with $\sigma_z = \sigma_\rho$, and no inverse is required. The application of equation (63) does not ensure that the resulting conductivities σ_1 and σ_2 are positive. In the case of negative conductivities, the assumed model or thickness is not valid.

4.2 Known top-layer conductvitity

If σ_1 is assumed, then the unknowns are σ_2 and d_1. The σ_2 can be eliminated from the equations in (56) to give

$$f(d_1) = \frac{R_\rho(d_1)}{R_z(d_1)} - \frac{\sigma_\rho - \sigma_1}{\sigma_z - \sigma_1} = 0, \tag{64}$$

which can be solved for d_1 using standard root finding methods. The ratio R_ρ/R_z is a monotonically increasing function in the range $[0, 1]$. Hence, for there to be a solution, we require that

$$0 \leq \frac{\sigma_\rho - \sigma_1}{\sigma_z - \sigma_1} \leq 1. \tag{65}$$

The first (positive) inequality tells us that if $\sigma_z > \sigma_1$ then $\sigma_\rho > \sigma_1$, or if $\sigma_z < \sigma_1$ then $\sigma_\rho < \sigma_1$. From the second (less than unity) inequality, if the bottom line is positive, then $\sigma_z > \sigma_1$ and hence $\sigma_z > \sigma_\rho$. Similarly if the bottom line is negative, then $\sigma_z < \sigma_1$ and hence $\sigma_z < \sigma_\rho$. If a root exists, it can be found by back substitution into one of the equations in (56).

4.3 Known bottom-layer conductivity

If σ_2 is assumed, then σ_1 and d_1 are unknown. Eliminating σ_1 from the equations in (56) gives

$$f(d_1) = \sigma_\rho - \sigma_z + R_z(d_1)(\sigma_2 - \sigma_\rho) + R_\rho(d_1)(\sigma_z - \sigma_2) = 0. \tag{66}$$

Again, this can be solved for d_1 using a standard root finder, and σ_1 found by back substitution. In the limit $d_1 \to 0$, $f(d_1) = 0$; however, this is not the required solu-

tion, as this reduces to the half-space case. The function $f(d_1)$ is more complicated and requires more analysis to determine when there is a solution. Writing

$$f(d_1) = \sigma_\rho - \sigma_z + R_z(d_1)\alpha + R_\rho(d_1)\beta, \tag{67}$$

where $\alpha = \sigma_2 - \sigma_\rho$, and $\beta = \sigma_z - \sigma_2$. Turning points of $f(d_1)$ can be found by setting $\mathrm{d}f(d_1)/\mathrm{d}d_1 = 0$, which can be solved using (59) and (60) to give a single turning point

$$d_1 = -\left(z_s + \frac{\beta}{\alpha\left[z_s + \sqrt{1+z_s^2}\right]}\right). \tag{68}$$

The only realistic turning points are for $d_1 > 0$, so

$$\frac{\beta}{\alpha} < -z_s\left(z_s + \sqrt{1+z_s^2}\right). \tag{69}$$

The sign of $f(d_1)$ prior to the turning point, can be ascertained by determining the slope of $f(d_1)$ at $d_1 = 0$. Specifically,

$$\frac{\mathrm{d}f(d_1)}{\mathrm{d}d_1}|_{d_1\to 0} = \frac{-\left[\alpha z_2\sqrt{1+z_s^2} + \alpha z_s^2 + \beta\right]}{(1+z_s^2)^{3/2}\left(1 + z_s(1+z_s^2)^{-1/2}\right)}. \tag{70}$$

The slope is positive if the term in square brackets is negative and negative if the term in square brackets is positive. If the term in square brackets is zero, the turning point is at $d_1 = 0$ and there are no other solutions. The value of the function $f(d_1)$ at $d_1 = \infty$ is $\sigma_\rho - \sigma_2$. Hence, there is a solution to equation (66) if:

1. the slope of $f(d_1)$ is positive at $d_1 = 0$, there is a turning point $d_1 \epsilon (0, \infty]$,and

$\sigma_\rho - \sigma_z$ is negative.

2. the slope of $f(d_1)$ is negative at $d_1 = 0$, there is a turning point $d_1 \epsilon (0, \infty]$,and $\sigma_\rho - \sigma_z$ is positive.

If there is no solution, then the other model is more appropriate.

4.4 Newtonian root finder

The way chosen to determine the parameters of the thick sheet over half space for the case of known bottom-layer conductivity in what follows is with the familiar Newton method

$$J_O(\sigma_1, \sigma_2, d_1)\overrightarrow{h} = -\overrightarrow{O}(\sigma_1, \sigma_2, d_1) \tag{71}$$

as applied to a system of non-linear equations for the σ_2 known case where:

$$\overrightarrow{h} = \begin{bmatrix} \Delta\sigma_1 \\ \Delta d_1 \end{bmatrix}, \; J_0 = \begin{bmatrix} \frac{\partial O_\rho}{\partial \sigma_1} & \frac{\partial O_\rho}{\partial d_1} \\ \frac{\partial O_z}{\partial \sigma_1} & \frac{\partial O_z}{\partial d_1} \end{bmatrix}, \tag{72}$$

so

$$\begin{bmatrix} \frac{\partial O_\rho}{\partial \sigma_1} & \frac{\partial O_\rho}{\partial d_1} \\ \frac{\partial O_z}{\partial \sigma_1} & \frac{\partial O_z}{\partial d_1} \end{bmatrix} \begin{bmatrix} \Delta\sigma_1 \\ \Delta d_1 \end{bmatrix} = - \begin{bmatrix} O_\rho - O_\rho^m \\ O_z - O_z^m \end{bmatrix} \tag{73}$$

which can be inverted to give an update

$$\begin{aligned} \Delta\sigma_1 &= \frac{\left(O_\rho - O_\rho^m\right)\frac{\partial O_z}{\partial d_1} - (O_z - O_z^m)\frac{\partial O_\rho}{\partial d_1}}{\frac{\partial O_\rho}{\partial d_1}\frac{\partial O_z}{\partial \sigma_1} - \frac{\partial O_\rho}{\partial \sigma_1}\frac{\partial O_z}{\partial d_1}} \\ \Delta d_1 &= \frac{(O_z - O_z^m)\frac{\partial O_\rho}{\partial \sigma_1} - \left(O_\rho - O_\rho^m\right)\frac{\partial O_z}{\partial \sigma_1}}{\frac{\partial O_\rho}{\partial d_1}\frac{\partial O_z}{\partial \sigma_1} - \frac{\partial O_\rho}{\partial \sigma_1}\frac{\partial O_z}{\partial d_1}}. \end{aligned} \tag{74}$$

The equation will iterate to a solution from a guess of the two unknowns where O_ρ^m and O_z^m are the measured response of the earth and O_ρ, O_z correspond to the model response for ρ and z components. The Jacobian matrix (J_0) can be modified to yield solutions for the σ_1, σ_2, and d_1 known cases. The root finding algorithm is sensitive to measurement noise, but this effect can be minimized by carefully levelling the input

data and dampening changes in the parameter at each iteration by multiplying by a small factor. In our work we found that multiplication by 0.05 resulted in stable estimates.

5 Field experiment, Russell South

5.1 Uranium exploration and geological setting

The Russell South property is located in the south eastern Athabasca Basin, which is notably prospective for uranium exploration. The basement below the Athabasca Basin is the Hearne craton, above which lies unconformably Proterosoic metasediment. Uranium deposits exist in the Athabasca Basin in the presence of structural complexity, through which fluids were permeated and uranium was deposited at economic grades in the form of uraninite. It is close to the unconformity between the Hearne and the Proterosoic metasediments that the deposits are normally found, often near a graphitic seam that continues down into the Hearne. In the deposit model there also exists a halo of alteration where the gangue rock has reacted with the same fluids to form clay. The thickness of the Proterosoic metasediment package can be up to 2 km, meaning that some deep deposits probably lie undiscovered Jefferson et al. (2007). At the Russell South property, the depth to the unconformety is approximately 100 m in the south, to 250 m in the north Robertshaw (2006).

Quaternary sediments exist and are likely to be the principal geological control on the topography. They exist in the form of lake sediments, moraines, eskers, and drumlins. Quaternary sediments are henceforth referred to as overburden because they have had no influence upon the genesis of uranium, and their variable thickness and geophysical properties could be an obstacle to geophysical methods of exploration. In particular, their variable thickness can have an impact on the gravity response that obscures the gravity response of the identifying alteration Darijani

(2019).

5.2 GEOTEM dataset

The GEOTEM airborne EM data set was collected between March 10th, 2005 and March 16th 2005 by Fugro Airborne Surveys on behalf of Roughrider Uranium Corporation using a modified Casa 212 aircraft. The detailed survey equipment specifications can be found in the report by Fugro, which was filed for assessment with the geological survey of Saskatchewan by Roughrider and is publicly available.

Figure 4 illustrates the transmitter current and x-, y- and z-component response as found in the Fugro report. Gate 1 is the on-time gate with the steepest primary response, and the time derivative will approximate a Dirac delta function, so it was the channel chosen for interpretation Smith (2000). Airborne EM has been used extensively in the Athabasca Basin to search for the graphite shear zones in the basement, and this was the purpose of the Russell South survey flown in 2005 with a line spacing of 300 m. As the graphite shear zones are very conductive, they are easily distinguishable in the off-time measurement gates. Because the goal of the survey was to measure conductive features in the off-time, little emphasis appears to have been put upon the leveling and filtering of the on-time collection windows. A triangular filter with a width of 91 points was applied to remove pendulum effects of bird swing. The emphasis of this step cannot be overstated, if ignored this noise signal upsets the stability of the newtonian root finder.

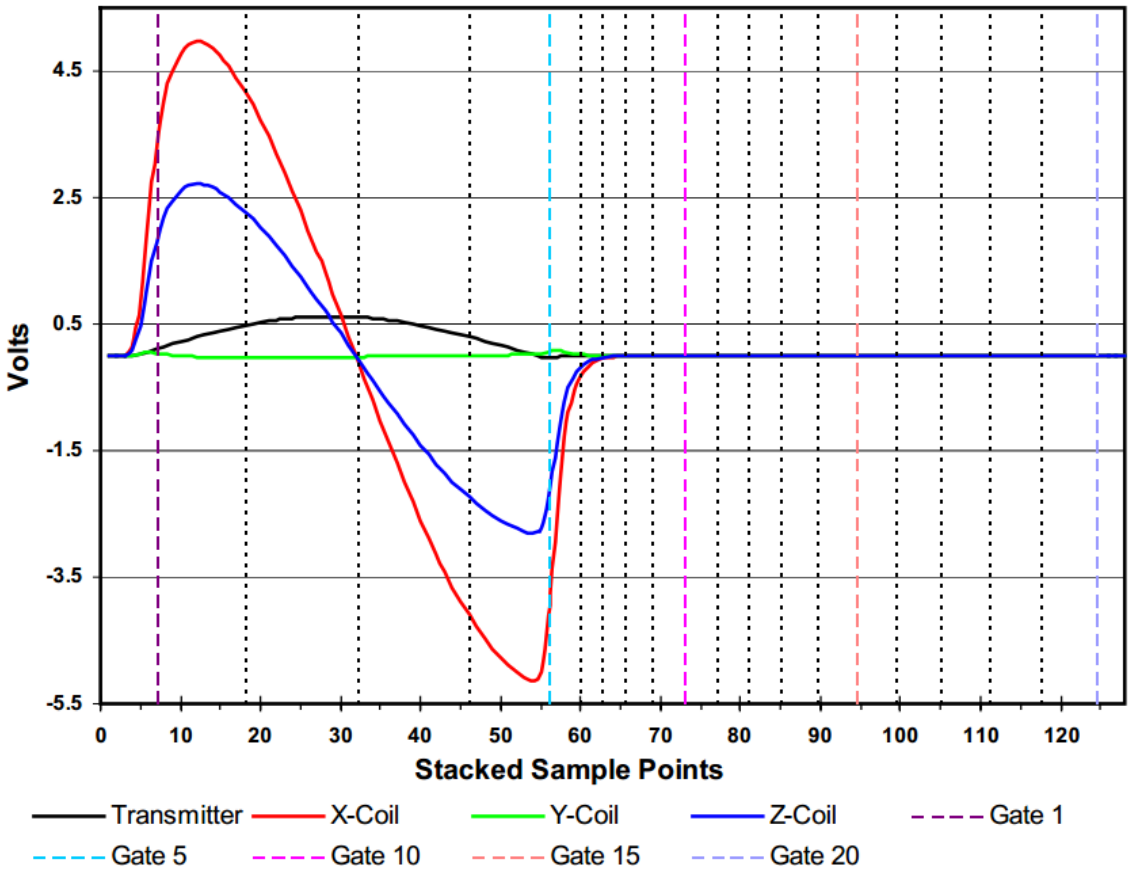

Figure 4: The primary field for x, y, and z components for on-time gates 1-5 and off-time gates 6-20, as presented by Fugro.

5.3 Inversion to sheet thickness

The inversion procedure described in sections 4.3 and 4.4 was applied to invert for sheet thickness and conductivity using the known half-space conductivity method. The half-space conductivity was estimated by comparing the x and z solutions for half-space conductivity. Those that were within 1% of each other were deemed to be valid estimates of half-space conductivity. We found that the half-space determined in this way was generally about 0.0003 S/m or less and the conductivity of the upper layer was generally greater than 0.0003 S/m, so we found it expedious to set the half-space conductivity everywhere to the average value of 0.00295 S/m. The inversion code was written in C and first tested to be self-consistent against synthetic models Bagley and Smith (2018), included below as an appendix. Once deemed internally consistent, it was then applied to the Russell South data set and the output imaged in Oasis Montaj. The processing and inversion steps are summarized by the flow chart presented in Figure 5.

The response in the z- and x-components are shown in Figure 6 and 7. These images were gridded using the minimum curvature method. The z and x components are similar, so the response is likely associated with large flat-lying features such as overburden. In the following, we have assumed that the x component is the ρ component. The radar altimeter on the GEOTEM aircraft (shown on Figure 8) is subtracted from the GPS height of the aircraft to create the digital terrain model (DTM), which is shown on Figure 9. Both Figures 8 and 9 are gridded using minimum curvature. The terrain model shows highs (red) running north-northeast, likely glacial features such as drumlins. The areas of low terrain (blue) appear in

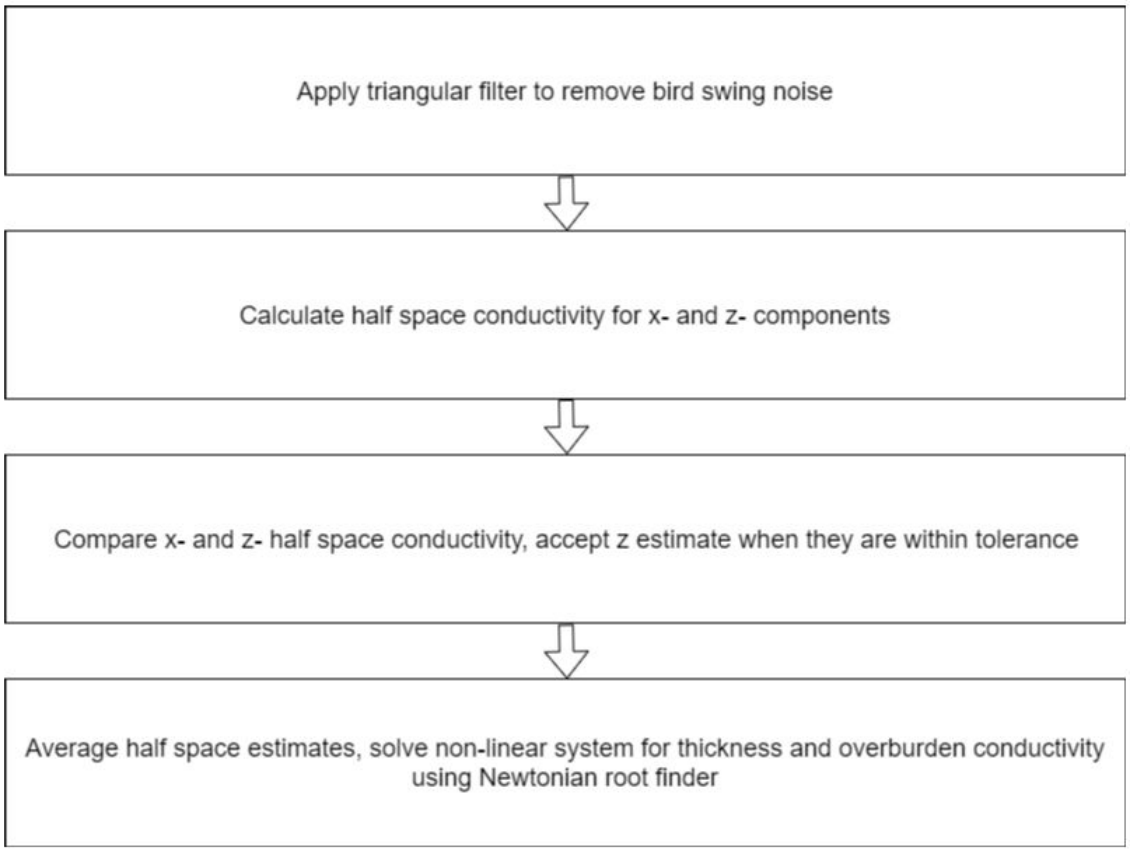

Figure 5: Flowchart summarizing processing and inversion steps.

many cases to have larger z- and x-component responses. These could be due to swamps or more conductive lacustrine sediments. Some of these trend in a different direction from the topography, for example a feature trending north-northwest from the southern apex of the survey area.

The parameters derived from the inversion, thick sheet conductivity and thickness are shown in Figures 10 and 11 respectively. These images were gridded using inverse distance squared weighting to minimize overshoot artifacts.

The elevation (above sea level) of the resistive half-space is shown on Figure 12. This shows highest elevations associated with the more conductive areas, although there are a number of differences, so there may be additional information in this image.

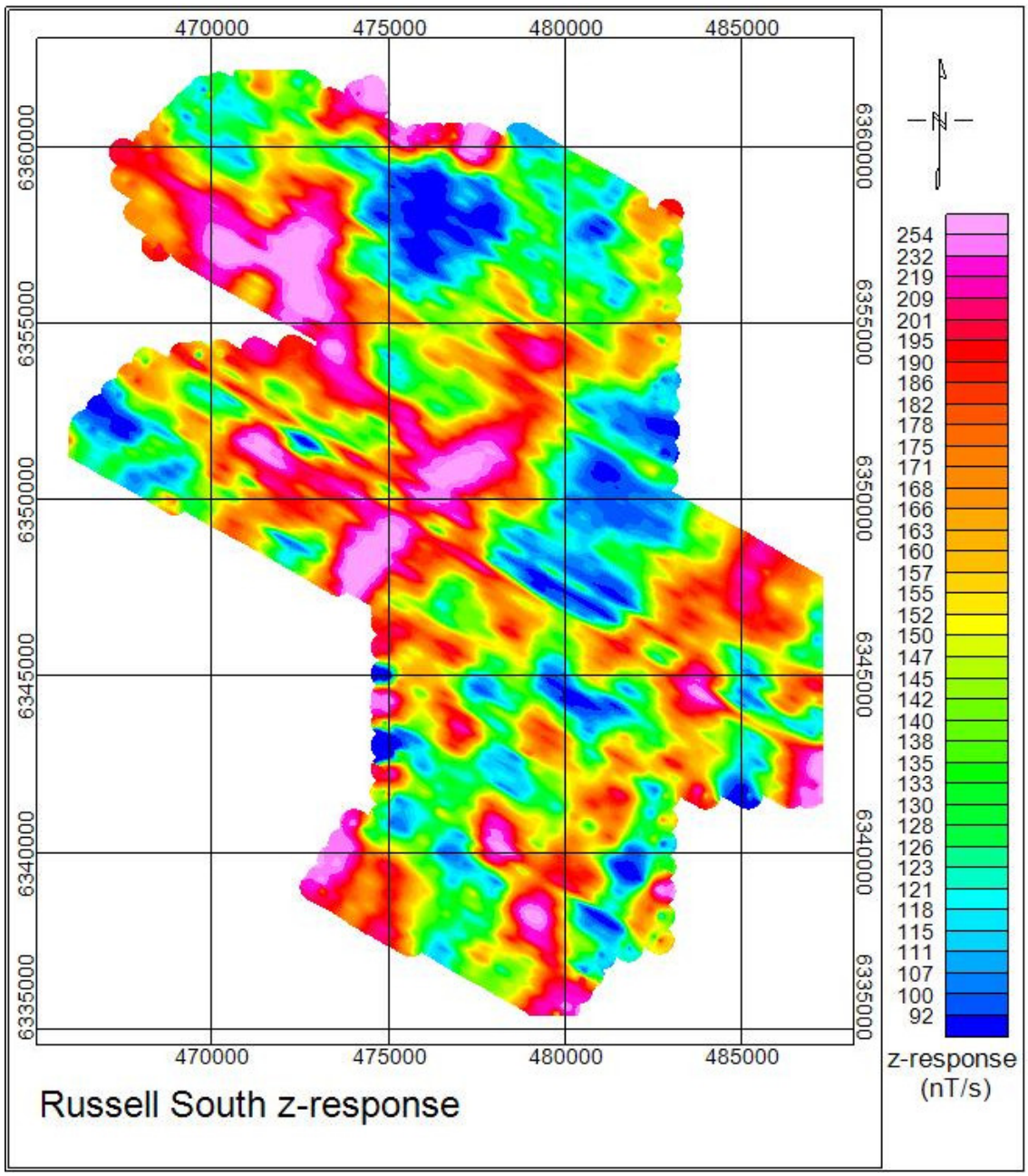

Figure 6: The z-response from the first measurement gate

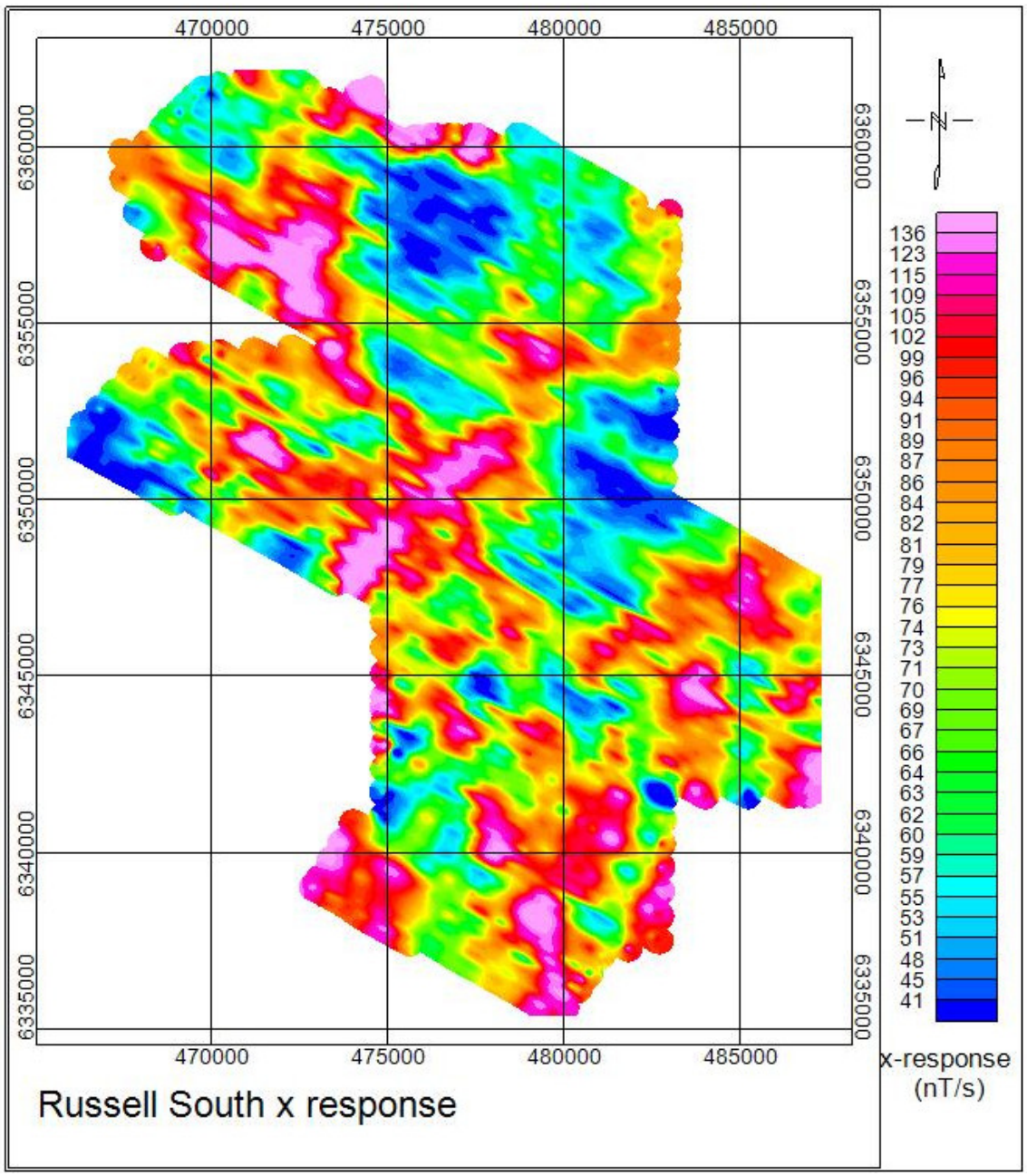

Figure 7: The x-response from the first measurement gate

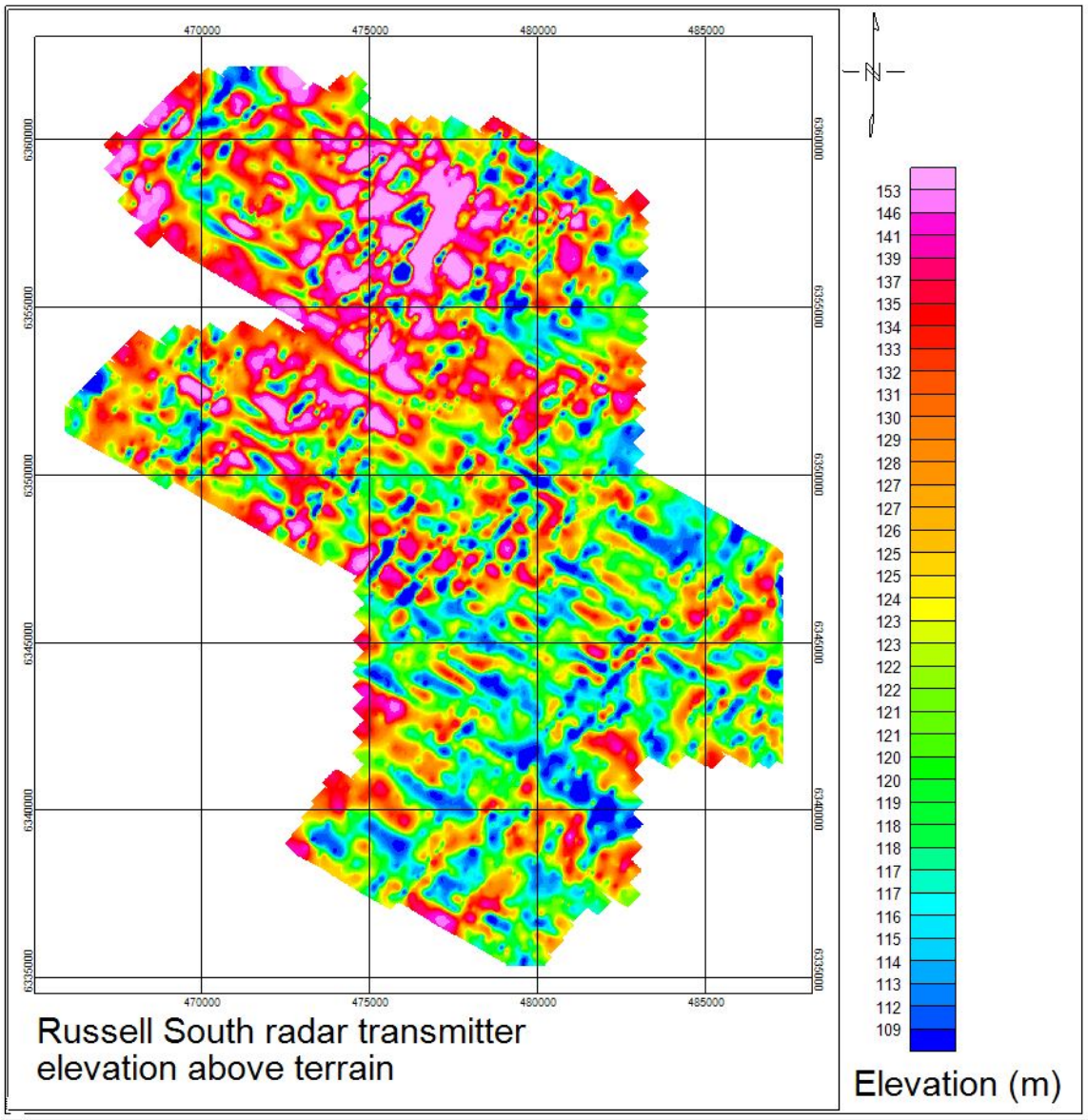

Figure 8: Aircraft altimeter height above terrain.

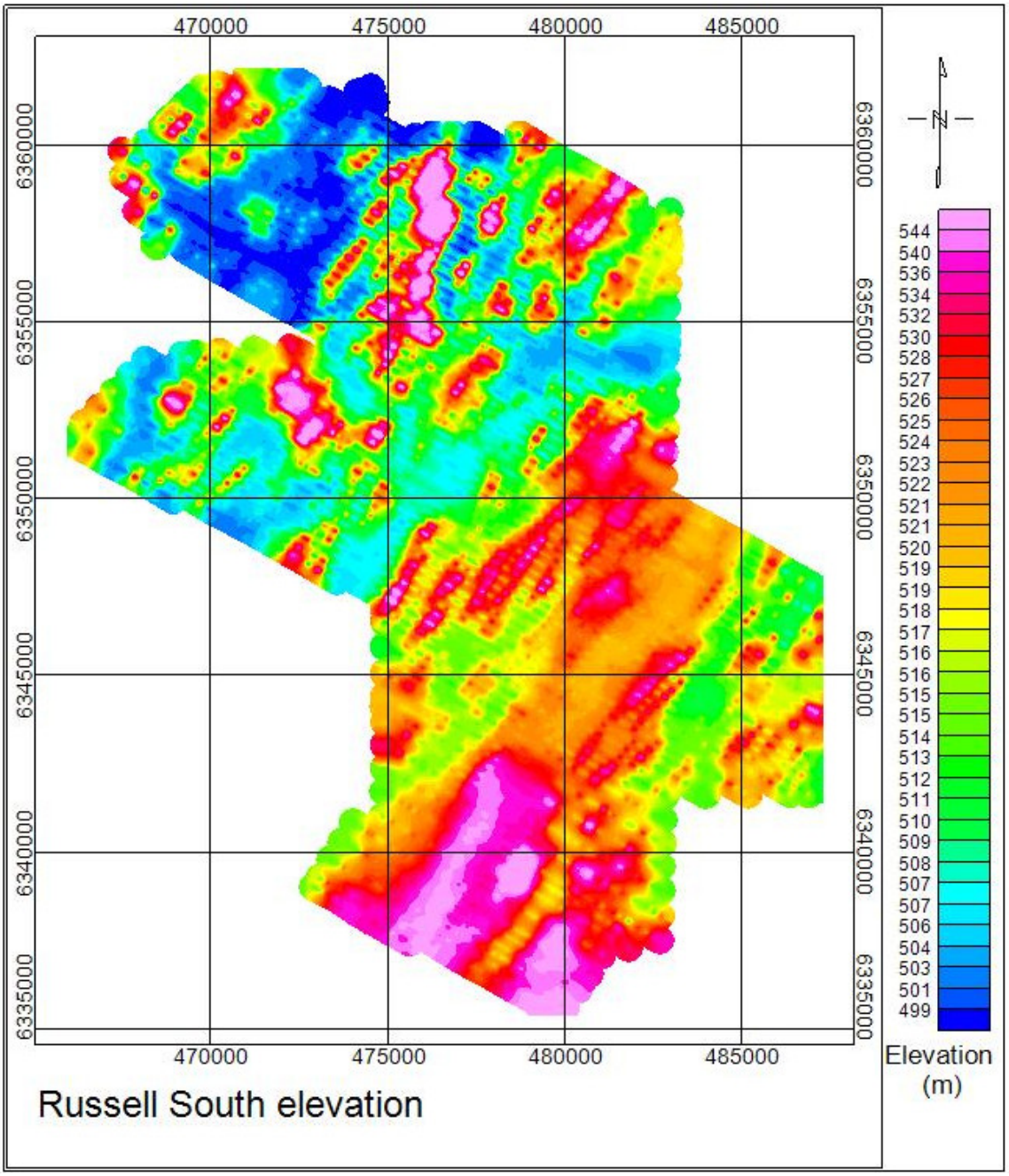

Figure 9: The digital terrain model of the area

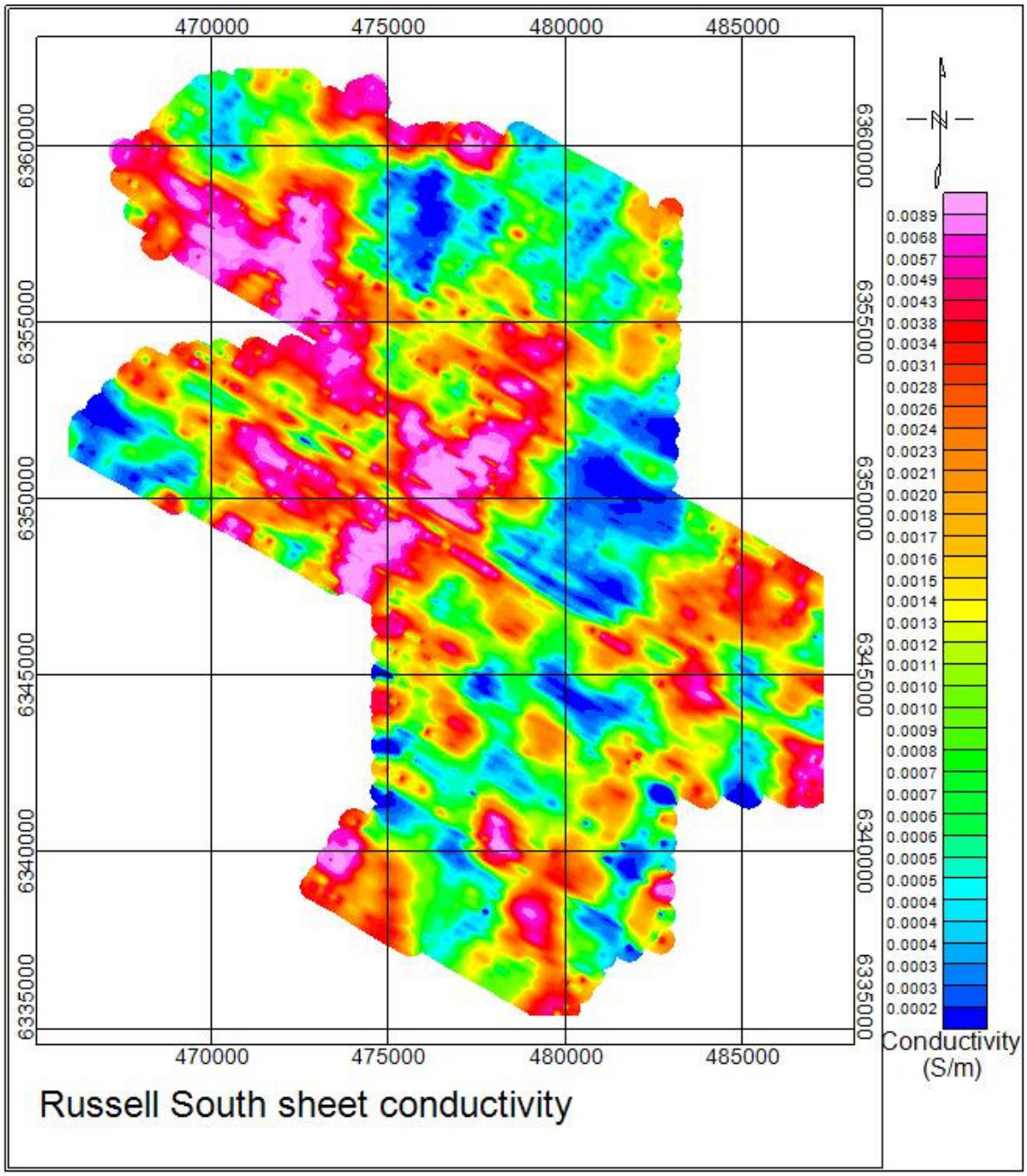

Figure 10: The thick-sheet conductivity representing overburden conductivity as determined by inversion with an estimated 0.000296 S/m half-space conductivity

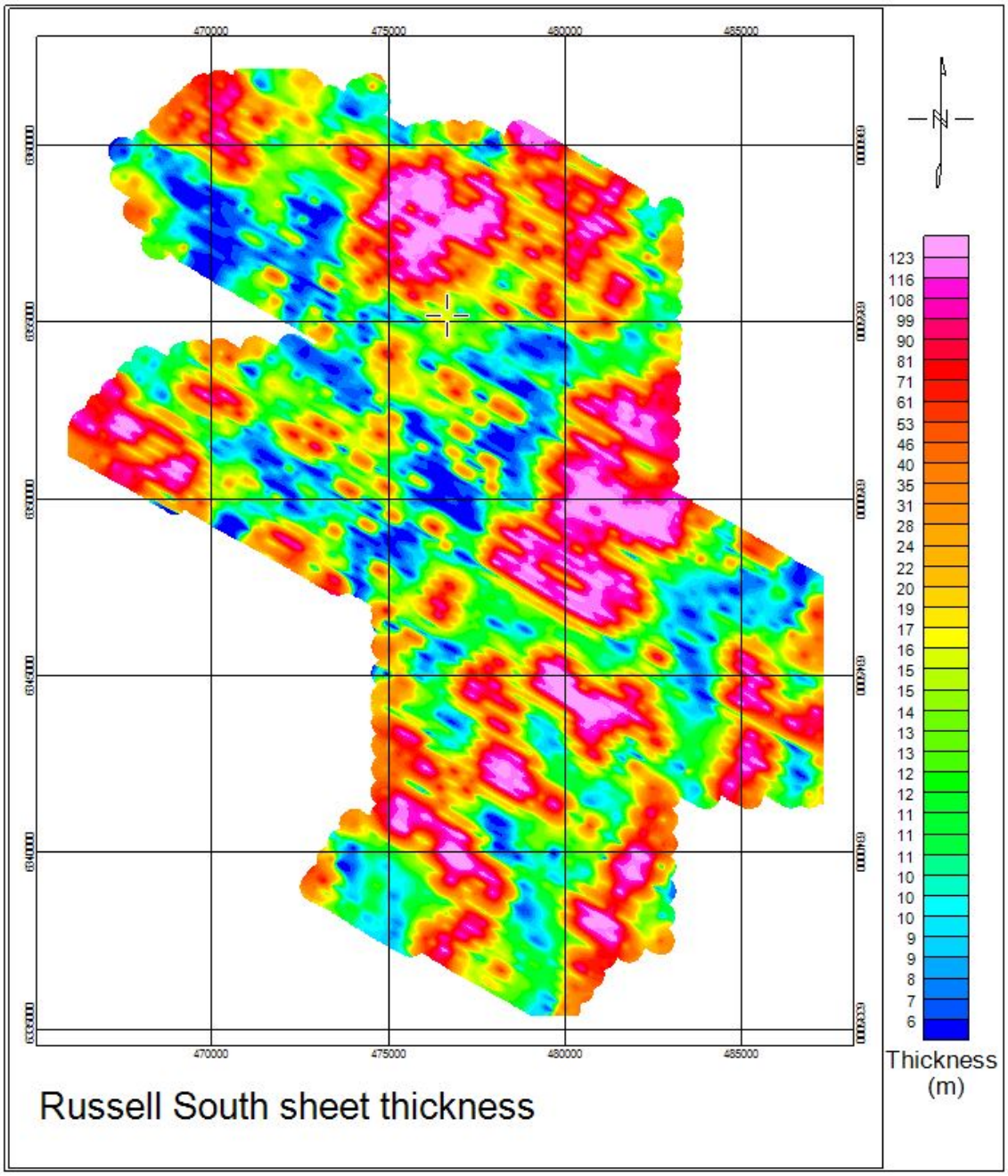

Figure 11: The thick-sheet thickness, representing the thickness of conductive overburden above a 0.000296 S/m half-space.

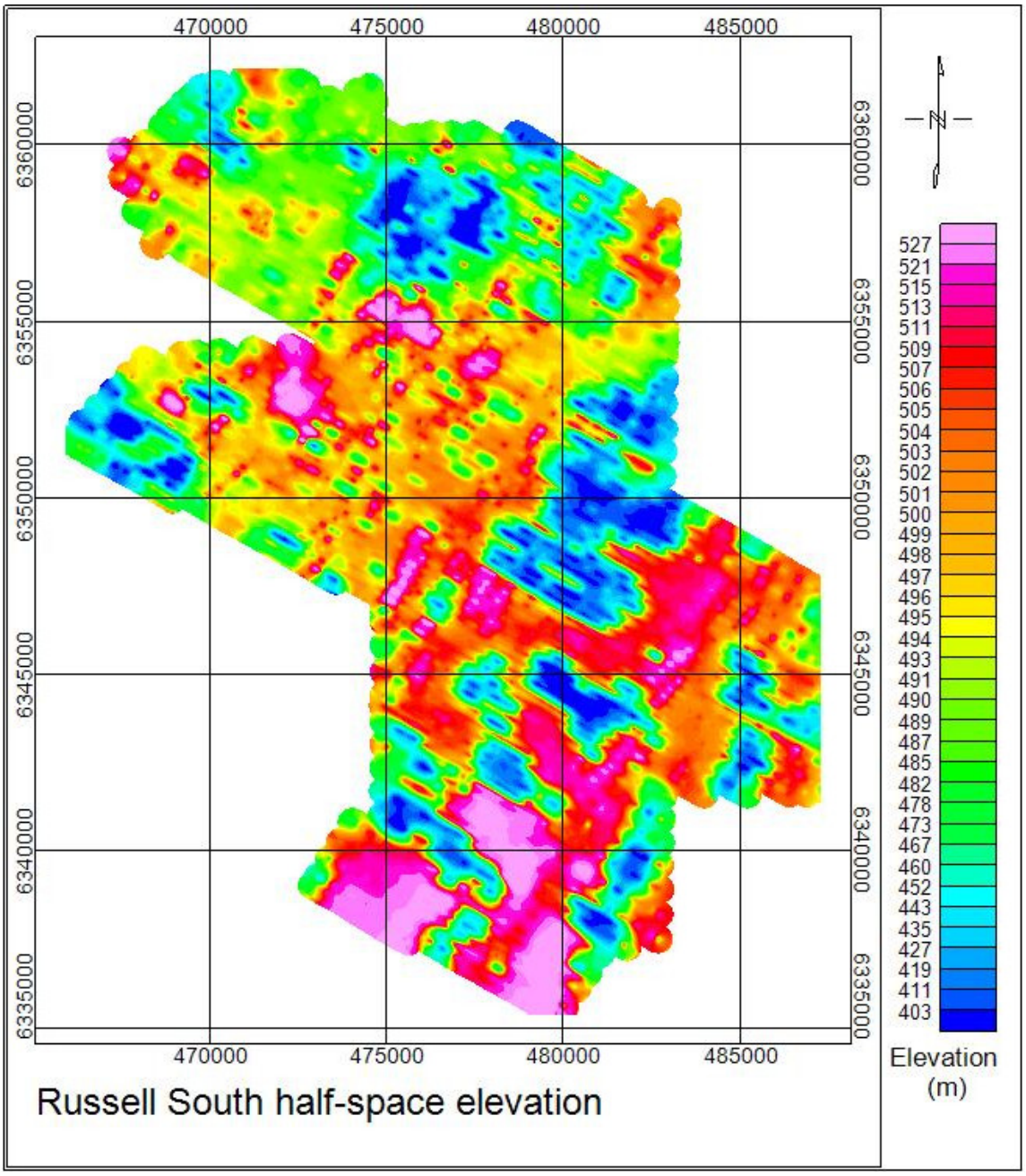

Figure 12: The half-space elevation, representing the elevation of the 0.000296 S/m half-space above sea level.

5.3.1 Comparison to casing depth of drilling

A drill hole database was obtained from the Geological Survey of Saskatchewan. The casing depth is presumed to closely correspond to the thickness of quaternary sediments, as they are usually unconsolidated and unstable. However, casing depth is an imperfect quality assessment tool for the following reasons: 1) borehole locations are sparse and non-random, generally being concentrated in more prospective areas; 2) casing is used where the rock is less competent, i.e. more fractured, but the AEM depth is based on conductivity; 3) some drillers may err on the side of safety and make the casing deeper than necessary; 4) the casing might be deeper than the overburden, due to the top of the bedrock being weathered below the overburden and less competent; 5) drill holes may be far from the flight lines and are poor estimates of the overburden thickness at the flight line location; 6) the location of the borehole might be incorrect, being enetered using an inconsistent datum (NAD 27 instead of NAD 83). The accuracy of this proxy may be within a few meters, as a weathered layer can exist at the top of the Proterosoic sediments. A comparison was made between the inverted sheet thickness and casing depth as a proxy for the overburden thickness (Figure 13). It can be seen that there are two population clusters. The first population is sparse, and the sheet thickness is about three times greater than the casing depth. The second population is tighter, and inverted sheet thickness is approximately half of that which has been estimated with casing depth.

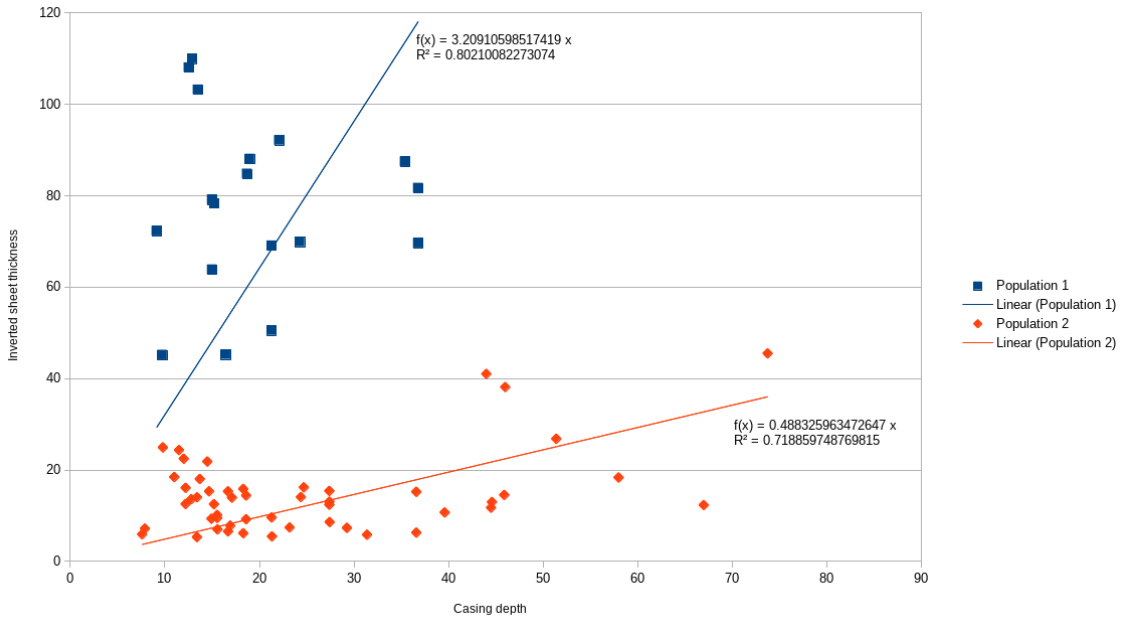

Figure 13: Comparison between inverted sheet thickness (y) and casing depth, a proxy for overburden thickness (x). Two distributions have been fitted using least squares to a line with a zero intercept.

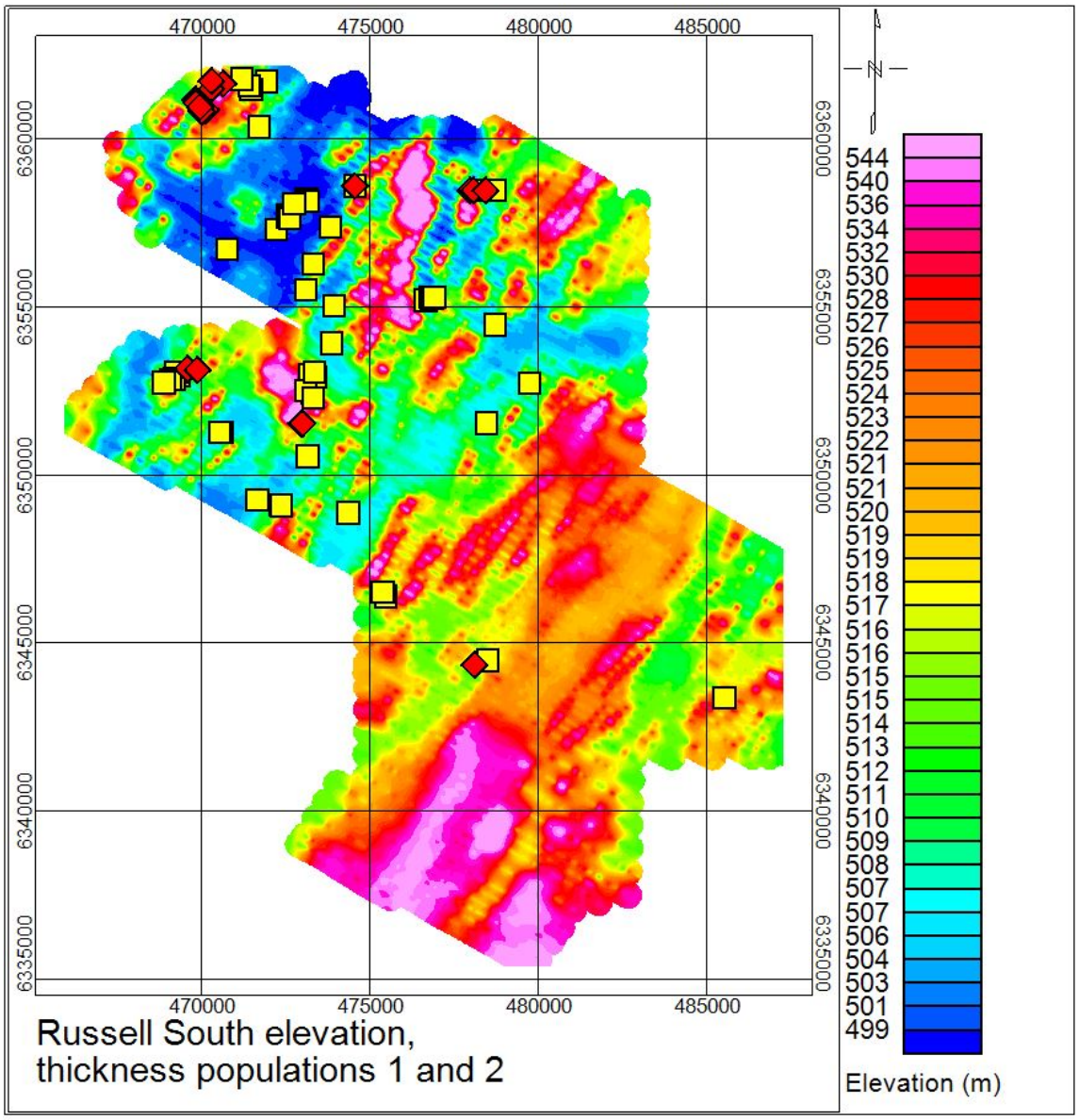

Figure 14: Distributions of population 1 (yellow filled squares) and population 2 (red filled squares) on map of elevation (DTM).

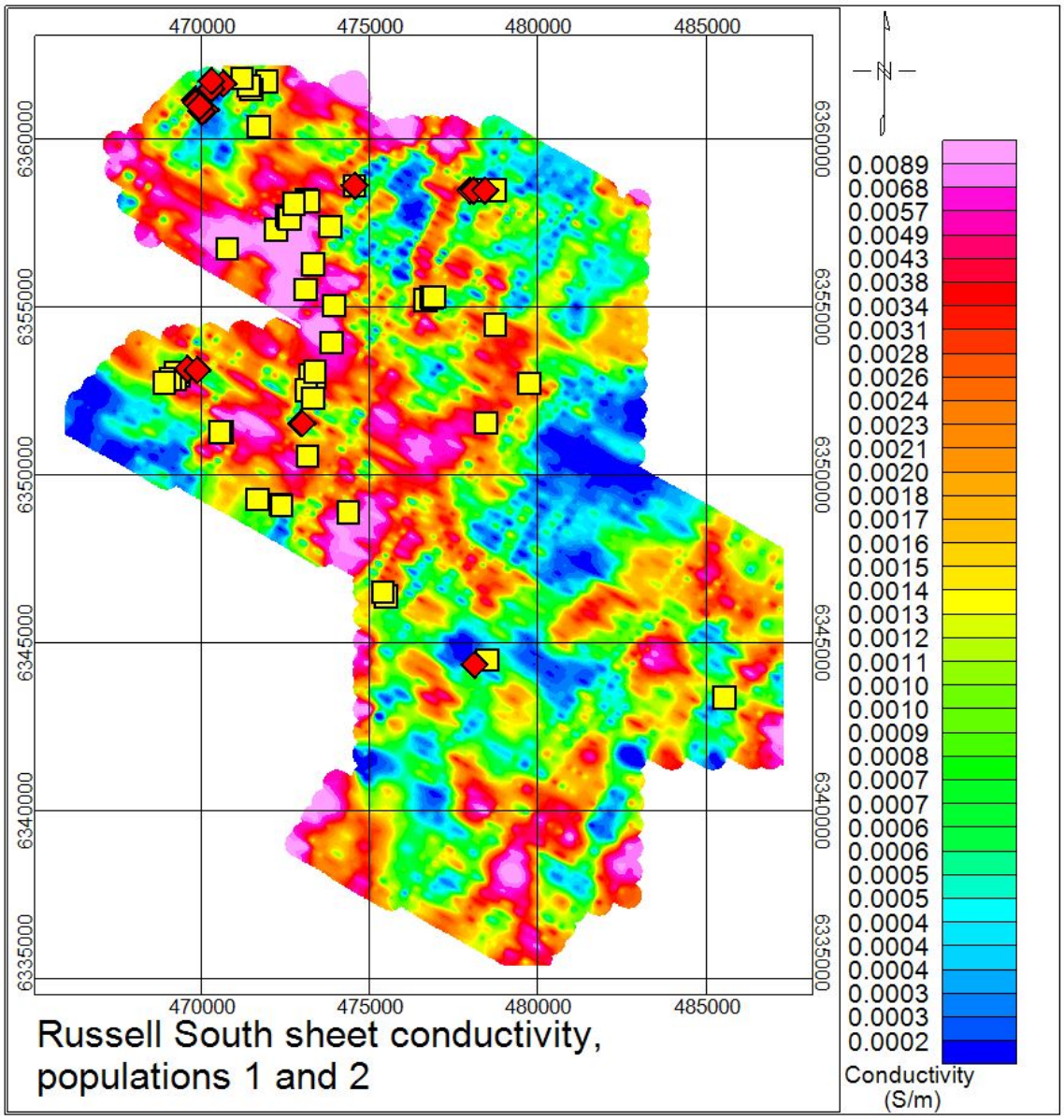

Figure 15: Distributions of population 1 (yellow filled squares) and population 2 (red filled squares) on map of thin-sheet conductivity derived from the x response

5.3.2 Comparison to topography

Casing depth is a useful proxy for the thickness of overburden, however the distribution of drilling is sparse. It is also presumed that the exploration drilling practice will minimize the meters of overburden drilled, for example drilling beside a drumlin rather than on top and through it, meaning that the sampling will be biased. Note that the drill locations in Figure 14 are away from the local peaks and in the local valleys, and there are no drill collars on the purple topographic highs. This means that the database is biased towards examples of low topography and thinner overburden (if the overburden thickness is assumed to be thicker below topographic highs). However, the EM will be sensitive to the nearby hills and result in a greater estimate of thickness. This might explain why some thickness estimates are too deep. Further, the casing depth will in many cases be greater than the overburden depth, as the decision may be made to make the casing deeper, so as to be sure the hole will not collapse in less consolidated material. Figure 16 compares the inverted sheet thickness to the terrain model for line 7101. It can be seen that some topographic features are coincident with strong features in the inverted sheet thickness, whereas some are not. The x-component response is also plotted on the profile.

On Figure 15 it can be seen that most of population 1 occur in areas where the conductivity is very small. These areas are often coincident with areas of high elevation (see Figure 14). It is likely that these high areas are less conductive because they are dry. As they are less conductive, the conductivity is close to that of the bedrock and the contrast between the overburden and bedrock is poor. In these areas the assumption of a conductor over a resistor will be poor; essentially, the geoelectric

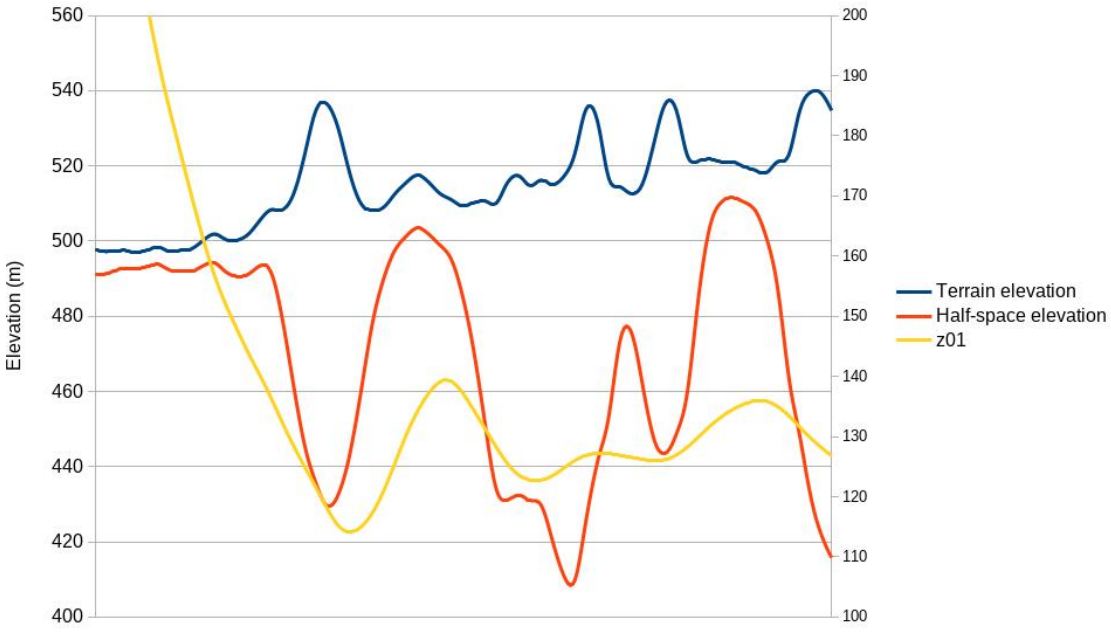

Figure 16: Comparison between the estimated elevation of the half-space (red), digital terrain model elevation (blue), and x response (yellow) for the 7101 survey line

structure is a half-space and the depth to the interface will be poorly constrained, so the algorithm seems to push the interface too deep. The second population is mostly in the areas where the conductivity is higher.

5.4 Discussion

Figures 7, 6 and 10 show that the conductivity of the thick sheet correlates strongly with the x and z response. Hence the magnitude of these responses is what determines the conductivity. The thickness of the sheet is a more complex relationship between the relative magnitude of the x and z response. When an x response is relatively strong with comparison to the z response, there exists a thick sheet on top of the half-space.

The digital terrain model in Figure 8 may be compared to the inverted sheet thickness in Figure 11. By comparison the inverted sheet thickness is smeared, with longer frequency features that are broad. Overall, the thickness generally shows that the thinner areas are associated with the more conductive features that have the stronger responses in the z- and x- component responses. Conversely the thicker areas are the areas with smaller responses and are more resistive. In these latter areas, a resistive half-space model might be more appropriate, so the thick layer model might not be appropriate and the depth poorly resolved (Bagley and Smith (2018); Appendix A).

The casing thickness from drilling was used as a proxy for overburden thickness, which was compared to the inverted sheet thickness in Figure 13. Neither population has a strong correlation to the sheet thickness, although the second population has a

much lower R^2 than the first. Figure 15 shows the location of population 1 with red diamonds and population 2 is shown with yellow squares. These two populations are interpreted to correspond to the resistive and conductive areas respectively. These conductive units might be clays or glaciolacustrine units within the overburden. The conductive units could be anywhere between the surface and the base of the overburden, which is consistent with the thickness being less than the overburden casing depth (the line with a slope of 1 on Figure 13). This interpretation that the estimates are related to conductive geological features within the overburden is reinforced by Figure 16, which shows the comparison between topography, x-component response, and the inverted sheet. If the primary control on topography was the overburden thickness and the bedrock surface was relatively flat, we would expect a thickness that mirrored the topography, however some topographic features are evident on the thickness trace, and others are missed entirely from the inverted sheet thickness. Those that are missed may represent highly resistive sands, and are perhaps below the limit of system detection. It is also worth considering that the genesis of glacial features like eskers and drumlins is uncertain, and that their genesis might have been a reflection of features in the paleotopography. If this was the case, then the thickness of overburden would not correlate with the topography.

6 Conclusion

The two component resistive-limit data allows two parameters of the ground to be resolved. Models which are completely described by two parameters are

1. the conductance and depth of a thin layer,

2. the depth to and conductance of a half-space,

3. the conductance of a thin layer at surface and the conductivity of an underlying half-space,

4. the conductivity and thickness of a thick layer at surface above a infinitely resistive basement

A two layer earth is completely described by three parameters (upper and lower conductivity and the depth to the interface). If one of the parameters is assumed, then the following models can be resolved

5. the conductivity above and below an interface at an assumed depth,

6. the depth to and conductivity of a layer below an upper layer of assumed conductivity and

7. the thickness and conductivity of a layer above a half-space of assumed conductivity.

The thick sheet, case 4), is a special case of case 7) where the lower half-space conductivity is assumed to be zero. Cases 4), 6) and 7) require that the root of an equation be solved to determine the depth to an interface. In case 2) the depth to a conductive half space can be compared to the height of the aircraft, and in this way a half-space conductivity can be determined with a degree of certainty. At locations where this situation occurs, this solution can then be used to estimate and

extrapolate the third parameter, the assumed value for the half-space below thick sheet model. The thick-sheet model can then be solved with an equation solver for sheet thickness and conductivity. In this way a third model parameter can be extracted from the two component data. When applied to real world data from the Athabasca Basin, the results were encouraging. However, where the response is small and noisy, the estimate of the thickness of the overburden was too deep and unreliable. Geospecially, these areas were generally coincident with hills, so it is hypothesized that the hills were dry and of low conductivity. Where the response was large the estimate was more reliable but generally too shallow, perhaps because the conductive material was above the overburden as estimated from the casing depth. Where signal is adequate, overburden thickness was distinct from the terrain with some features shared between the two.

References

Annan, A., Smith, R., Lemieux, J., O'Connell, M., and Pedersen, R. (1996). Resistive-limit time-domain AEM conductivity. *Geophysics*, 61:93–99. doi: 10.1190/1.1443960. 1, 2, 3, 3.1

Bagley, T. and Smith, R. (2018). Estimating overburden thickness in resistive areas from two-component airborne em data. *SEG Technical Program Expanded Abstracts*, pages 1893–1897. doi: 10.1190/segam2018-2998300.1. 5.3, 5.4

Darijani (2019). personal communication. This is a reference to his PhD thesis, which will be available soon. 5.1

Edwards, R. and Cheesman, S. (1987). Two-dimensional modeling of a towed transient magnetic dipole-dipole sea floor EM system. *Journal of Geophysics*, 61:110–121. doi: 10.1190/1.1442296. 4, 4

Grant, F. and West, G. (1965). *Interpretation theory in applied geophysics*. International series in the earth sciences. McGraw-Hill. doi: 10.1017/s0016756800050627. 1

Jefferson, W, C., Thomas, D., Gandhi, S, S., Ramaekers, P., Delauney, G., Brisbin, D., Cutts, C., Portella, P., and Olson, R, A. (2007). Unconformity-associated uranium deposits of the Athabasca Basin, Saskatchewan and Alberta. *Geological Survey of Canada*, 588:23–67. doi: 10.4095/223744. 5.1

McNeill, J. (1980). Electromagnetic terrain conductivity measurements at low in-

duction numbers. Technical note tn-6., Geonics Ltd. http://www.geonics.com/html/technicalnotes/tn6.pdf[Accessed: 2019.07.01]. 1, 4, 4.1, 4.1, 4.1

Parker, R. (1977). The fréchet derivative for the one-dimensional electromagnetic induction problem. *Geophys. J. R. Astr. Soc*, 49:543–547. doi: 10.1111/j.1365-246x.1977.tb03723.x. 4

Robertshaw, P. (2006). Report on a 2005 geotem survey Russell South property, northern Saskatchewan on behalf of Roughrider Uranium corp. Technical report, Robertshaw Geophysics Ltd. 5.1

Smith, R. (2000). The realizable resistive limit: a new concept for mapping geological features spanning a broad range of conductivities. *Geophysics*, 65:1124–1127. doi: 10.1190/1.1444805. 1, 5.2

Smith, R. (2001). On removing the primary field from fixed-wing time-domain airborne electromagnetic data: some consequences for quantitative modelling, estimating bird position and detecting perfect conductors. *Geophysical Prospecting*, 49:405–416. doi: 10.1046/j.1365-2478.2001.00266.x. 1

Smith, R., Edwards, R., and Buselli, G. (1994). An automatic technique for presentation of coincident-loop, impulse response, transient, electromagnetic data. *Geophysics*, 59:1542–1550. doi: 10.1190/1.1443543. 4, 4

Smith, R. and Lee, T. (2002). Using the moments of a thick layer to map the conductance and conductivity from airborne electromagnetic data. *Journal of Applied Geophysics*, 49:173–183. doi: 10.1016/S0926-9851(01)00112-4. 1

Spies, B. (1989). Depth of investigation in electromagnetic sounding. *Geophysics*, 59:1542–1550. doi: 10.1190/1.1442716. 4

Wait, J. (1982). *Geoelectromagnetism*. Academic Press. 1, 2, 2, 3.1, 3.2

Ward, S. (1966). Electromagnetic theory for goephysical applications in mining geophysics ii. *Soc. Expl. Geophys.*, pages 10–196. doi: 0.1190/1.9781560802716.ch2a. 2

Appendices

A Appendix 1

Estimating overburden thickness in resistive areas from two-component airborne EM data

Thomas Bagley and Richard Smith, Laurentian University

Summary

An overburden with variable thickness can obscure the response of underlying geophysical features. For example, the gravity response of an increased thickness of low-density overburden might not be distinguishable from a deeper sandstone hydrothermally altered to clay. When the overburden is conductive, it's thickness can be determined from the rate of decay of the off-time airborne electromagnetic data. However, the off-time decay of a thin or resistive overburden is small and difficult to measure. Previous studies have used the on-time resistive-limit response of a single component to successfully map apparent ground conductance in resistive areas. Quantitative resistive-limit models exist for thin-sheet, half-space, thin-sheet over half-space, and thick-sheet over half-space models. This study uses horizontal and vertical component data to estimate the thickness (and conductivities) of a two layered model across the survey profile.

Introduction

This study of overburden thickness has been conceived for application in the Athebasca Basin. The Ahtebasca Basin is known for its endowment of uranium deposits, which may be associated with graphitic conductors that are often easily detectable by airborne electromagnetic methods and many surveys have been conducted for this purpose. However, graphitic conductors exist in the absence of the economic mineral systems, and some of these systems exist in absence of graphitic conductors. The deposits are also charactarized by a low density hydrothermal clay alteration. Thus, deposits may exist at depth in the absence of graphitic conductors, and they may be detectable by gravity methods. In order to remove the masking effect of changes in the thickness of low-density overburden on gravity data, we are investigating the ability of resistive limit AEM to determine the thickness of the overburden.

The Athebasca Basin is comprised of the Athebasca Group metasediments up to 1400 m thick unconformably on top of metamorphic basement (Robertshaw, 2006). The resistivity of the Athebasca Group metasediments was estimated to be 10^4 Ωm by Smith (2010), and is thus transparent to electromagnetic surveying. The resistivity contrast with the basement below may be as high as 10^4 Ωm (Smith, 2010). The off-time response from the overburden is usually too rapid for reliable interpretation. Smith (2000) showed that quadrature on-time measurements can be inverted to conductivity and on-time data greatly improves measurement sensitivity for highly resistive provinces. This study aims to build upon this work and develop a resistive-limit, thick-sheet model to estimate overburden thickness in the Athebasca Basin.

Resistive-limit solutions for half-space and thick-sheet cases

Annan et al. (1996) showed that the conductivity of a half-space σ can be derived from the measured on-time resistive-limit window O_i of the ith component of temporal width ε and geometric factor G

$$\sigma=\epsilon\frac{O}{G}. \tag{1}$$

For a thin sheet (TS) overburden layer of thickness d_1 and conductivity σ_1 overlying a half-space of conductivity σ_2 we have

$$\begin{pmatrix}\sigma_1 d_1\\ \sigma_2\end{pmatrix}=\frac{1}{G_x^{TS}G_z^H-G_z^{TS}G_x^H}\begin{pmatrix}G_z^H & -G_x^H\\ -G_z^{TS} & G_x^{TS}\end{pmatrix}\begin{pmatrix}\epsilon O_x\\ \epsilon O_z\end{pmatrix}, \tag{2}$$

where G_i^{TS} and G_i^H are geometric factors for the thhin-sheet and half-space models. Finally for a thick-sheet over a half-space, we have (Bagley, 2019)

$$O_i=\left[\sigma_1\left(1-R_i(d_1)\right)+\sigma_2 R_i(d_1)\right]\frac{G_i^H}{\epsilon}, \tag{3}$$

where $R_i(d_1)$ is a non-linear geometry factor for the thick-sheet conductivity. For this model there are two measurements, but three unknowns, so a unique solution does not exist. However, an estimate for the thickness (d_1) can be obtained if the conductivity of the bottom layer can be estimated in some way (for example, by assuming lateral continuity).

A half-space solution exists for both the *x* and *z* components independently. Therefore, it may be tested for validity by comparing one against the other. McNeil (1980) showed that the *z*-component is more sensitive than *x* to deeper structures (figure 1), so the z-component is assumed to be a more reliable estimate of half-space conductivity at depth. A half-space consistent with the *x*- and *z* components may represent an exposure of bedrock, or that the overburden conductivity is equal to the bedrock conductivity $\sigma_1/\sigma_2=1$. In either case, if the half-space

conductivity from the x and z- components is near equal then it is deemed to be a valid estimate of half-space conductivity σ_2.

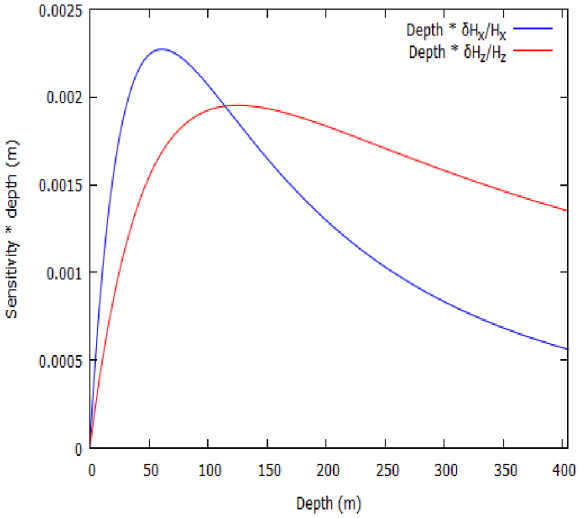

Figure 1 *System sensitivity depth for standard GEOTEM configuration.*

When the half-space conductivity σ_2 is known, the thick sheet response (equation 3) may have a unique solution for the conductivity and thickness of the overburden. Using a Taylor expansion we can write the familiar

$$J\vec{h} = -\vec{O}, \qquad (4)$$

where J is the Jacobian matrix containing the derivatives of the x and z responses with respect to σ_1 and d_1, $\vec{h}$ is a vector of σ_1 and d_1, and $\vec{O}$ is the vector of the difference between the measured response and the response from an initial guess for the x and z-component.

Synthetic example

Synthetic data was generated using equation (3). The profile was generated using the thick-sheet model for a range of thick-sheet conductivities from 0 to 0.1 S/m, and a half-space conductivity fixed at 0.02 S/m. In figure 2, the thicknesses step from 10 (models 1 to 10) up to 120 m (models 90 to 100). Gaussian noise of differing levels can be added to the model data and lower layer conductivity to test the robustness of the inversion to measurement noise.

An inversion algorithm was then designed to seek the nearest valid half-space solution. A valid half-space was deemed to be where the x- and z-component estimates for σ_2 differ by less than 1%. The half-space conductivity was then used as an estimate of lower half-space conductivity σ_2. Sheet thickness and conductivity were then solved for iteratively in neighboring samples using Newton's Method. The result from this algorithm are presented in figures 3 for d_1 and 4 for σ_1, superimposed onto the known synthetic model parameters (figure 2).

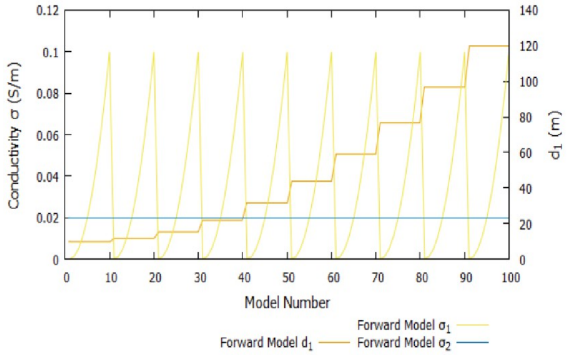

Figure 2 *Synthetic conductivity and depth profile of overburden model over 0.2 S/m half-space.*

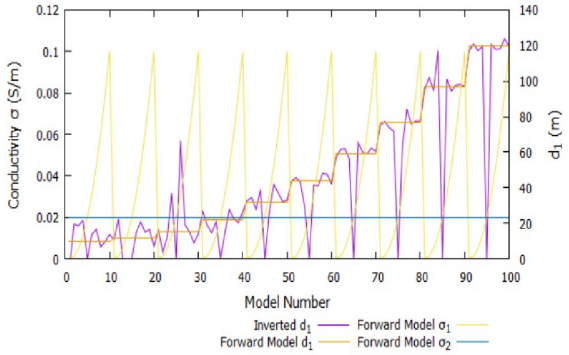

Figure 3 *Inversion of synthetic model for thickness and forward model parameters with Gaussian 1% half-space conductivity error and 1% measurement error.*

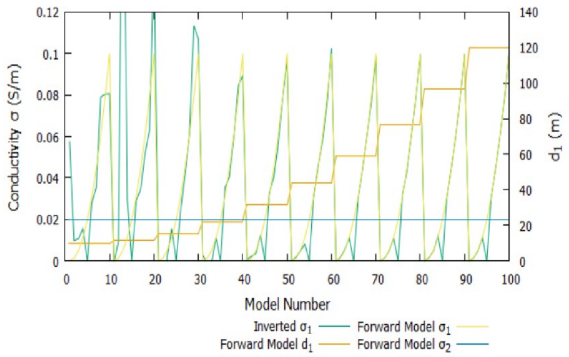

Figure 4 *Inversion of synthetic model for thick-sheet conductivity and forward model parameters with Gaussian 1% half-space conductivity error and 1% measurement error.*

Noise Sensitivity Analysis

The inversion of synthetic data was tried for different combinations of 1, 5, and 10% measurement errors, and 1% and 5% half-space conductivity error. The new combinations are shown in figures 5 to 10, where the depth and conductivities are plotted on top of the parameters that were used to generate the forward model. Because the error added is Gaussian, outliers may exist beyond two standard deviations from the mean at a rate of 4.2%, so 4 to 5 occurrences can be expected in each plot.

Larger uncertainties exist when the sheet is thinner or the conductivity of the upper layer is less than the halfspace, which is attributable to the system not being sensitive to thin or resistive layers. Referring back to figure 1, it can be seen that the GEOTEM system sensitivity sharply increases up to 40 m with x being more sensitive. Consequently, the response declines sharply as depth becomes shallow and small measurement or half-space conductivity errors may cause large discrepancies in the inverted thickness and conductivity.

In figure 3, it can be seen that 1% noise in measurement and half-space conductivity corrupts the depth estimate when the overburden thickness is less than approximately 20 m and the resistivity of the overburden is less than the half-space. Above 20 m, the thickness can be resolved above noise with confidence. It can be seen in figure 3 that the depth profile drops to zero in the middle of each thickness step. This is where the upper and lower conductivities are approximately equal and there is no contrast. Consequently, the response is equal to that of a half-space which has zero thickness.

Figures 5 and 6 show the case of 5% Gaussian measurement error added to the x and z response. Similarly to the 1% example shown in figures 3 and 4, the inverted thickness drops to zero during each step when there is no conductivity contrast between the sheet and the half-space. There is much noise in the earlier section and thickness can only be estimated with a reasonable uncertainty above 60 m, where the inversion resembles the forward model more closely. In the 5% half-space conductivity error examples shown in figures 7 and 8, measurement error has a less damaging effect to the inversion as the thickness and overburden conductivity can be estimated with confidence above 30 m.

Figures 9 to 10 show 10% measurement error added to the x and z components. In this case, the inversion cannot find a solution at some low thickness points, and has large uncertainty even at large thicknesses.

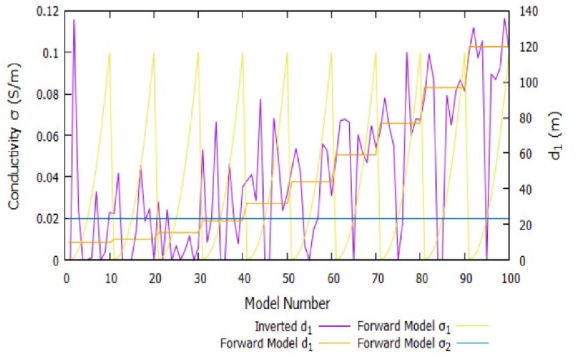

Figure 5 *Inversion of synthetic model for thickness and forward model parameters with Gaussian 1% half-space conductivity error and 5% measurement error.*

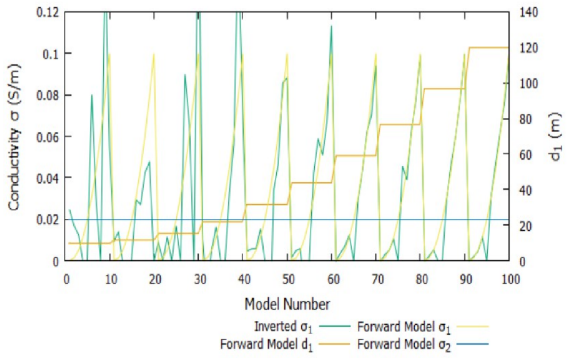

Figure 6 *Inversion of synthetic model for thick-sheet conductivity and forward model parameters with Gaussian 1% half-space conductivity error and 5% measurement error.*

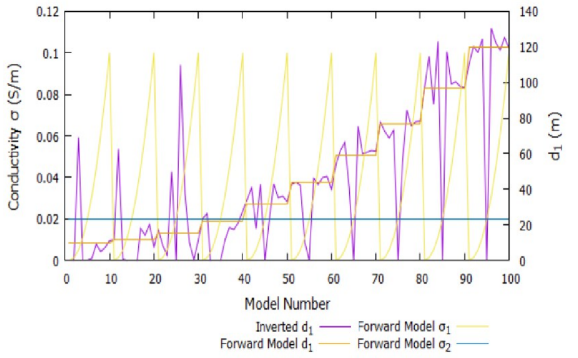

Figure 7 *Inversion of synthetic model for thickness and forward model parameters with Gaussian 5% half-space conductivity error and 1% measurement error.*

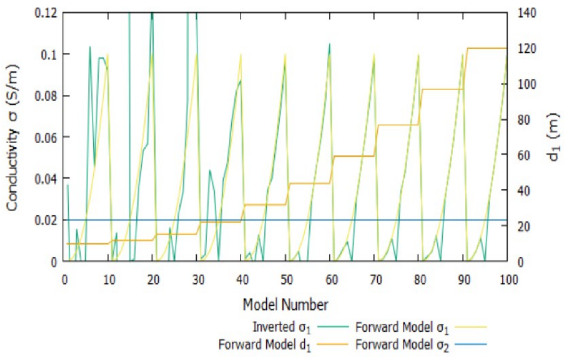

Figure 8 *Inversion of synthetic model for thick-sheet conductivity and forward model parameters with Gaussian 5% half-space conductivity error and 1% measurement error.*

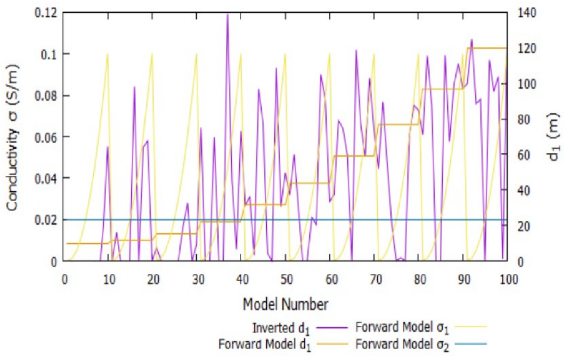

Figure 9 *Inversion of synthetic model for thickness and forward model parameters with Gaussian 1% half-space conductivity error and 10% measurement error.*

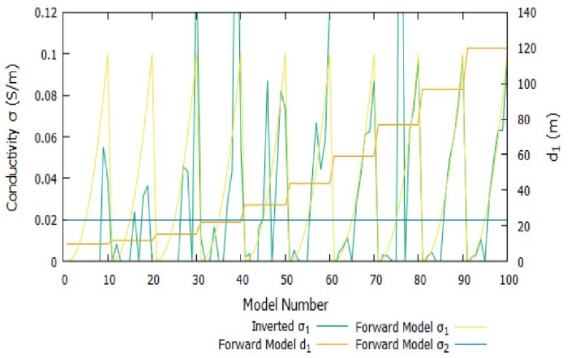

Figure 10 *Inversion of synthetic model for thick-sheet conductivity and forward model parameters with Gaussian 1% half-space conductivity error and 10% measurement error.*

Future Work

Several approaches will be taken to improve the inversion. Firstly, the inversion may be made in combination with other models. For example, in the case when the sheet is thin, a thick-sheet model could be replaced with a thin conductive sheet model (equation 2) to estimate the conductance and depth of the sheet from the *x* and *z* components. Secondly, the thin-sheet conductivity depth solution can be tested for validity by comparing the inverted *x* and *z* components, then used to estimate the thickness of a thick sheet with the assumption of a homogeneous thin-sheet conductivity, where the thickness will be twice the depth from the surface and the conductivity will be the conductance divided by the thickness. In order to test if the algorithm is getting stuck in a local minimum, experiments will be made replacing Newton's with Gauss-Newton or Marquardt inversion. These methods minimize least squared-error, and can use several samples to determine the best fitting solution.

Finally, the inversion will be applied to GEOTEM survey data from the Athebasca Basin made public available by the Geological Survey of Saskatchewan. It will then be compared to local drill core logs.

Conclusion

Synthetic thick-sheet over half-space modeling suggests that two component airborne electromagnetic data can be inverted to overburden thickness. The inversion was done by comparing every x- and z-component half-space solution. Those that differed by less than 1% were deemed to be a valid estimate of the lower half-space conductivity. Then, assuming conductivity was laterally continuous, the thickness of the overlying sheet was determined using Newton's method. Noise sensitivity analysis indicated that inversion to thickness is robust for measurements with 5% Gaussian noise, if the sheet is thicker than 60 m. For measurements with 10% Gaussian noise, the inversion was corrupted and only trended weakly with sheet thickness. Work will be done to incorporate the thin-sheet over half-space model into the inversion algorithm, as this might improve performance at smaller thicknesses. Gauss-Newton and Marquardt algorithms will be investigated to test if the corruption at small thicknesses is the result of non-linear local minimum effects.